Decreased Activity of the *Ghrhr* and *Gh* Promoters Causes Dominantly Inherited GH Deficiency

Daisuke Ariyasu[1,2], Emika Kubo[1], Daisuke Higa[1], Shinsuke Shibata[3], Yutaka Takaoka[4], Michihiko Sugimoto[1], Kazunori Imaizumi[5], Tomonobu Hasegawa[6], and Kimi Araki[1,7]

[1]Division of Developmental Genetics, Institute of Resource Development and Analysis, Kumamoto University, Kumamoto, Japan
[2]Graduate School of Medicine, Keio University, Tokyo, Japan
[3]Electoron Microscope Laboratory, Keio University School of Medicine, Tokyo, Japan
[4]Division of Medical Informatics and Bioinformatics, Kobe University Hospital, Hyogo, Japan
[5]Department of Biochemistry, Graduate School of Biomedical and Health Sciences, Hiroshima University, Hiroshima, Japan
[6]Keio University School of Medicine, Tokyo, Japan
[7]Center for Metabolic Regulation of Healthy Aging, Kumamoto University Faculty of Life Sciences, Kumamoto, Japan

To whom correspondence should be addressed: Kimi Araki, Division of Developmental Genetics, Institute of Resource Development and Analysis, Kumamoto University, 2-2-1, Honjo, Kumamoto, 860-0811, Japan. Tel.: +81.96.373.6598; Fax: +81.96.373.6599 E-mail: arakimi@gpo.kumamoto-u.ac.jp

Running title: ER-localized mutant GH decreases GH1 mRNA

Abstract

Isolated growth hormone deficiency type II (IGHD2) is mainly caused by heterozygous splice-site mutations in intron 3 of the *GH1* gene. A dominant negative effect of the mutant growth hormone (GH) lacking exon 3 on wild-type GH secretion has been proposed; however, the molecular mechanisms involved are elusive. To uncover the molecular systems underlying GH deficiency in IGHD2, we established IGHD2 model mice, which carry both wild-type and mutant copies of the human *GH1* gene, replacing each of the endogenous mouse *Gh* loci. Our IGHD2 model mice exhibited growth retardation associated with intact cellular architecture and mildly activated ER stress in the pituitary gland, caused by decreases in the growth hormone releasing hormone receptor (*Ghrhr*) and *Gh* gene promoter activities. Decreases in *Ghrhr* and *Gh* promoter activities were likely caused by reduced levels of nuclear CREB3L2, which was demonstrated to stimulate the activity of the *Ghrhr* and *Gh* promoters. This is the first *in vivo* study revealing a novel molecular mechanism of GH deficiency in IGHD2, representing a new paradigm, differing from widely accepted models.

Key Words: dominant negative effect/ endoplasmic reticulum stress/ growth hormone/ growth hormone releasing hormone receptor/ isolated growth hormone deficiency type II

Introduction

Isolated growth hormone deficiency type II (IGHD2) is a dominantly inherited growth hormone (GH) deficiency, first described in 1994, and mainly caused by heterozygous splice-site mutations in intron 3 of the *GH1* gene (Binder & Ranke, 1995; Cogan et al, 1994). The wild-type *GH1* allele transcript includes 5 exons and produces a 22-kDa wild-type GH protein; however, the mutant *GH1* allele transcript generates a 17.5-kDa exon 3 deletion-mutant GH (Δ3 GH), as a result of in-frame skipping of exon 3. The fact that patients harboring a deletion in one *GH1* allele exhibit normal stature indicates that a single wild-type *GH1* allele is sufficient to produce normal levels of wild-type GH secretion (Akinci et al, 1992); however, patients with IGHD2 have low serum concentrations of wild-type GH, despite having a wild-type *GH1* allele. Thus, it has been suggested that Δ3 GH exerts a dominant negative effect on wild-type GH secretion; however, the precise molecular mechanisms involved have remained elusive for more than 20 years.

Several *in vitro* studies have demonstrated that Δ3 GH is not secreted extracellularly (Graves et al, 2001; Iliev et al, 2005; Kannenberg et al, 2007; Mullis et al, 2002; Salemi et al, 2006), suggesting that the dominant negative effect of Δ3 GH is exerted within somatotropic cells of the pituitary, where GH is generated. Generally, mutant proteins exert dominant negative effects on secretory pathways of wild-type factors at the protein level (Deladoey et al, 2001; Ito et al, 1999; Jacobson et al, 1997), which has led many researchers to focus on wild-type and Δ3 GH protein interactions, such as heterodimer formation; however, no study has yet demonstrated definitive evidence of heterodimers comprising wild-type and Δ3 GH proteins. At present, it is widely accepted that Δ3 GH itself is not harmful to somatotroph (Graves et al, 2001), and that wild-type GH contributes to the degradation of Δ3 GH via protein interactions, leading to impairment of the wild-type GH secretory pathway (Kannenberg et al, 2007; McGuinness et al, 2003).

In contrast, previous *in vitro* studies revealed that Δ3 GH localizes to the endoplasmic reticulum (ER), due to its aberrant protein structure (Graves et al, 2001; Salemi et al, 2006), and is degraded by the proteasome (Ariyasu et al, 2013; Kannenberg et al, 2007), indicating that Δ3 GH potentially causes ER stress in the somatotroph. We previously demonstrated the involvement of ER stress and apoptosis in IGHD2, using rat GH4C1 cells stably expressing wild-type GH and Δ3 GH (Ariyasu et al, 2013), indicating that Δ3 GH itself impairs ER functions *in vitro*, without the involvement of wild-type GH, inconsistent with the widely accepted hypothesis described above.

Since GH secretion is regulated by growth hormone releasing hormone (GHRH) signaling, it is important to establish a usable model that includes the hypothalamus-pituitary axis. One *in vitro* study has authentically mimicked the hypothalamus-pituitary axis (Petkovic et al, 2010); however, *in vivo* animal models are imperative to clarify the molecular mechanisms involved in the GH deficiency of IGHD2. McGuinness *et al.* established Δ3 GH transgenic mice and reported that they exhibited widespread pituitary damage and severe macrophage invasion (McGuinness et al, 2003). This mouse model had been the sole *in vivo* model used to represent the human IGHD2 phenotype. *In vivo* studies have been performed using this model, including Δ3 GH knockdown by shRNA (Lochmatter et al, 2010), and altering splicing efficiency using butyrate (Miletta et al, 2016), which ameliorated impaired GH secretion; however, the mechanisms underlying IGHD2 have not been determined *in vivo* (Miletta et al, 2017).

To clarify the molecular processes causing impaired GH secretion in IGHD2, we established IGHD2 model mice by exchanging endogenous mouse *Gh* genes for the

human wild-type *GH1* (*wtGH1*) and mutant *GH1* (*Δ3GH1*; generates Δ3 GH) genes, using the 'gene exchange system' previously reported by our laboratory (Araki et al, 2002). Our IGHD2 model mice demonstrated significant growth failure, associated with a marked decrease in *wtGH1* mRNA, and no apoptosis was detected in the pituitary glands, despite the clear growth retardation phenotype.

Here, we show that Δ3 GH decreases transcription from the growth hormone releasing hormone receptor (*Ghrhr*) gene promoter, which has a fundamental role in somatotroph proliferation, as well as *GH1* gene transcription, leading to impaired GH production before birth in IGHD2 model mice. These decreases in promoter activity were mediated by a reduction in nuclear CREB3L2, one of the Creb3 family of bZip transcription factors, which was found to stimulate transcription from the *Ghrhr* and the *Gh* promoters coordinately with POU class 1 homeobox 1 (POU1F1). This is the first *in vivo* study to reveal a novel molecular mechanism underlying GH deficiency in IGHD2, and provides a new paradigm, different from the widely accepted model.

Results

IGHD2 model mice exhibited mild growth retardation

To establish a mouse model that authentically demonstrates the Δ3 GH-mediated dominant negative effect observed in IGHD2, one each of the mouse endogenous *Gh* gene alleles was exchanged for the human *wtGH1* and *Δ3GH1* genes, using the gene exchange system previously reported by our laboratory (Araki et al, 2002). Briefly, we inserted a *neoR* gene cassette, flanked by a left-element mutated *lox*JT15 and *lox*P site, at the *Gh* gene locus by homologous recombination, producing a mouse *Gh* knock-out (KO) allele (Gh^{-}) (Fig EV1A and C). Then, we constructed gene exchange vectors, containing right-element mutated *lox*KR3 and the *wtGH1* or *Δ3GH1* genes, followed by a puromycin resistance gene and the *lox*P site (Fig EV1A and C). The *neoR* gene cassette was exchanged for the *wtGH1* or *Δ3GH1* genes using Cre-mediated recombination (Fig EV1A and B). Since recombination between *lox*JT15 and *lox*KR3 produced a *lox* site with both sides mutated, which is resistant to Cre-mediated excision, we were able to efficiently generate recombined embryonic stem (ES) cell clones (Fig EV1A) (Araki et al, 2002).

Schematic representations of the original mouse endogenous *Gh* allele (Gh^{+}), KO allele (Gh^{-}), and exchanged human *GH1* alleles (Gh^{wtGH1} or $Gh^{\Delta 3GH1}$) are presented in Fig 1A. By crossing $Gh^{+/-}$, $Gh^{+/wtGH1}$, and $Gh^{+/\Delta 3GH1}$ mice, we successfully established $Gh^{wtGH1/wtGH1}$ mice (human healthy control model), $Gh^{wtGH1/-}$ mice (*GH1* heterozygous

deletion model), $Gh^{wtGH1/\Delta3GH1}$ mice (IGHD2 model), and $Gh^{-/-}$ mice (*GH1* homozygous deletion model). The body weights and body lengths of these model mice are shown in Fig 1B and C. $Gh^{-/-}$ mice demonstrated severe postnatal growth retardation, associated with serum insulin-like growth factor 1 (IGF-1) levels below the detection range, indicating that, as in humans, postnatal growth in mice is dependent on GH activity (Fig 1B–E). $Gh^{wtGH1/wtGH1}$ and $Gh^{wtGH1/-}$ mice showed longitudinal growth and serum IGF-1 levels comparable with those of $Gh^{+/+}$ mice, suggesting that the human wild-type GH molecule is capable of binding the mouse GH receptor and producing IGF-1, and that one exchanged human wild-type *GH1* allele is sufficient for IGF-1-mediated longitudinal growth in mice (Fig 1B–E). $Gh^{wtGH1/\Delta3GH1}$ mice exhibited mild growth retardation, associated with significantly reduced serum IGF-1 values, which were intermediate between those of $Gh^{wtGH1/wtGH1}$ and $Gh^{-/-}$ mice (Fig 1B–E). These data indicate that $Gh^{wtGH1/\Delta3GH1}$ mice successfully demonstrate the dominant negative effect of Δ3 GH, and that the growth retardation of $Gh^{wtGH1/\Delta3GH1}$ mice is caused by impaired GH activity.

We also established $Gh^{mGh/\Delta3GH1}$ mice, in which the mouse *Gh* gene was inserted at the endogenous mouse *Gh* locus, using the gene exchange system in a similar way to that used to obtain $Gh^{wtGH1/\Delta3GH1}$ mice (Fig EV1A). $Gh^{mGh/\Delta3GH1}$ mice also demonstrated growth failure, as for $Gh^{wtGH1/\Delta3GH1}$ mice, although $Gh^{+/\Delta3GH1}$ mice did not (Fig EV1E). The phenotypic discrepancy between $Gh^{+/\Delta3GH1}$ and $Gh^{mGh/\Delta3GH1}$ mice was attributable to a significant difference in the abundance of mRNA transcribed from the endogenous and exchanged *Gh* alleles, as demonstrated by qRT-PCR (Fig EV1F). In this study, we used mouse lines in which both alleles were exchanged for human *GH1* genes, because the transcriptional efficiencies of the *wtGH1* and *Δ3GH1* alleles were basically equivalent in human IGHD2 patients. These decreases in transcriptional efficiency of the exchanged human *GH1* genes did not cause the growth failure in $Gh^{wtGH1/wtGH1}$ mice (Fig 1B and C), and IGF-1 levels in $Gh^{wtGH1/wtGH1}$ mice were comparable with those in $Gh^{+/+}$ mice (Fig 1D), indicating that *wtGH1* mRNA expression levels were sufficient for production of human wild-type GH protein, required for the IGF-1-mediated longitudinal growth of mice.

The growth retardation of $Gh^{wtGH1/\Delta3GH1}$ mice is caused by decreased *wtGH1* mRNA expression

We evaluated the expression levels of wild-type and Δ3 GH proteins in pituitary glands at 4 weeks of age, the period in which $Gh^{wtGH1/\Delta3GH1}$ mice demonstrated significant growth retardation, based on their growth curves (Fig 1B and C). Immunoblotting showed significant decreases in the content of the 22 kDa wild-type GH

in whole *Gh*$^{wtGH1/\Delta 3GH1}$ pituitary, compared with *Gh*$^{wtGH1/wtGH1}$ and *Gh*$^{wtGH1/-}$ pituitaries (Fig 2A left and B), indicating that the growth retardation of *Gh*$^{wtGH1/\Delta 3GH1}$ mice was caused by impaired GH production in the somatotroph. Δ3 GH expression was barely detected by long exposure (Fig 2A right), despite comparable affinities of the anti-GH antibody for wild-type and Δ3 GH proteins (Fig EV2A). Immunostaining revealed that both the wild-type GH content in each somatotroph and the number of somatotrophs were reduced in *Gh*$^{wtGH1/\Delta 3GH1}$, compared with *Gh*$^{wtGH1/wtGH1}$ pituitaries (Fig 2C).

Since we had demonstrated impaired production of wild-type GH in *Gh*$^{wtGH1/\Delta 3GH1}$ pituitary, we next evaluated *GH1* transcript levels. Using whole pituitary glands from 4-week-old animals, RT-PCR detecting both the *wtGH1* and *Δ3GH1* transcripts, with a sense primer in exon 1 and an antisense primer in exon 5, revealed markedly decreased *wtGH1* transcript levels in the *Gh*$^{wtGH1/\Delta 3GH1}$ pituitary, compared with those in *Gh*$^{wtGH1/wtGH1}$ and *Gh*$^{wtGH1/-}$ pituitaries (Fig 2D). qRT-PCR analysis, detecting the *wtGH1* mRNA alone, using a sense primer in exon 3 and an antisense primer spanning exons 3 and 4, also demonstrated that the abundance of the *wtGH1* mRNA in *Gh*$^{wtGH1/\Delta 3GH1}$ pituitary was approximately one sixth of that in *Gh*$^{wtGH1/wtGH1}$ pituitary in 4-week-old animals (Fig 2E). Decreases in *wtGH1* mRNA levels in *Gh*$^{wtGH1/\Delta 3GH1}$ pituitaries were demonstrated from embryonic day E19.5 to 4 weeks of age (Fig 2F), suggesting that GH production in *Gh*$^{wtGH1/\Delta 3GH1}$ pituitaries was already impaired before birth. *In situ* hybridization analysis to detect *wtGH1* mRNA using an RNA probe for *GH1* exon 3, in E19.5 and 4-week-old pituitaries, revealed that both the abundance of *wtGH1* mRNA in each somatotroph and the number of somatotrophs were decreased in *Gh*$^{wtGH1/\Delta 3GH1}$ pituitaries, consistent with the results of immunostaining (Fig 2C and G). These data indicate that the impaired production of wild-type GH in *Gh*$^{wtGH1/\Delta 3GH1}$ pituitary is caused by a decrease in *wtGH1* mRNA.

RT-PCR showed that levels of the *wtGH1* and *Δ3GH1* transcripts were comparable (Fig 2D); however, immunoblotting revealed that expression of the Δ3 GH protein was drastically reduced compared with that of wild-type GH protein in *Gh*$^{wtGH1/\Delta 3GH1}$ pituitaries (Fig 2A). These data indicate that Δ3 GH is degraded in the somatotroph, and that wild-type GH is not involved in the degradation, inconsistent with the currently accepted hypothesis. Thus, to evaluate whether wild-type GH preferentially interacts with Δ3 GH, 3-D protein structures of wild-type and Δ3 GH were analyzed under pH conditions in the ER and docking simulation analysis was conducted using ZDOCK (Chen et al, 2003; Nakamura et al, 2017). The average binding affinity score for heterodimers of wild-type and Δ3 GH was significantly lower than that for the wild-type GH homodimer (Table 1), indicating that wild-type and Δ3 GH heterodimer

formation is unlikely to be involved in impaired GH secretion in IGHD2.

Electron microscopy reveals markedly decreased numbers of secretory vesicles and enlarged ER in *Gh*$^{wtGH1/\Delta3GH1}$ pituitaries

Considering the possibility that somatotroph loss due to apoptosis, necrosis, and inflammation, contribute to the decrease in *wtGH1* mRNA described above, we conducted histological evaluation of pituitary glands (Fig 3). Stereomicroscopic analysis of four-week-old *Gh*$^{wtGH1/\Delta3GH1}$ pituitaries revealed a slightly atrophic and semi-translucent appearance, which was intermediate between those of *Gh*$^{wtGH1/-}$ and *Gh*$^{-/-}$ mice, consistent with the decreased somatotroph number in *Gh*$^{wtGH1/\Delta3GH1}$ mice described above (Fig 3A); however, the decrease in somatotroph number was not caused by somatotroph loss, since hematoxylin-eosin staining demonstrated that the cellular architecture was intact, with no signs of necrosis or inflammation. Further, analysis by TdT-mediated dUTP nick end labeling (TUNEL) assay revealed that the decrease in the *wtGH1* mRNA in *Gh*$^{wtGH1/\Delta3GH1}$ mice was not associated with apoptosis (Fig 3B).

The absence of somatotroph loss in *Gh*$^{wtGH1/\Delta3GH1}$ mice led us to evaluate the characteristics of the cellular organelles in pituitary glands using transmission electron microscopy (TEM). TEM images of 4-week-old *Gh*$^{wtGH1/wtGH1}$ pituitary glands showed intact cell organelles, including appropriately developed rough ER, and many secretory vesicles containing mature wild-type GH protein (Fig 3C). In contrast, images of *Gh*$^{wtGH1/\Delta3GH1}$ pituitary glands revealed a clear decrease in the number of secretory vesicles, abnormal enlargement of the rough ER, and protein aggregates in the cytosol (Fig 3C). To evaluate the impact of Δ3 GH itself on cellular morphology, we obtained *Gh*$^{\Delta3GH1/-}$ mice by crossing *Gh*$^{wtGH1/-}$ and *Gh*$^{wtGH1/\Delta3GH1}$ animals. In contrast to the current understanding that Δ3 GH itself is not harmful to somatotroph, TEM images of *Gh*$^{\Delta3GH1/-}$ pituitaries revealed extreme enlargement of the rough ER and protein aggregates in the cytosol, whereas such abnormalities were not visible in *Gh*$^{-/-}$ pituitaries (Fig 3D). The observed protein aggregates were connected to the ER (Fig 3E), suggesting that the proteins accumulated in the ER were retro-translocated to the cytosol, leading to aggregate formation. These data led us to confirm the cellular localization of Δ3 GH by immunofluorescence analysis. Using *Gh*$^{wtGH1/\Delta3GH1\text{-}myc}$ mice, expressing Δ3 GH with a C-terminal myc tag (Fig EV1A), Δ3 GH was also demonstrated to localize within the ER *in vivo* (Fig 3F).

To evaluate the contents of the protein aggregates in the cytosol, we dissociated *Gh*$^{wtGH1/\Delta3GH1}$ anterior pituitary cells and separated them into soluble and insoluble

fractions, in the presence or absence of treatment with the proteasome inhibitor, MG132, and evaluated the distributions of wild-type and Δ3 GH by immunoblotting, because several studies have demonstrated that cytosolic protein aggregates have low solubility (Ariyasu et al, 2013; Imai et al, 2001; Kannenberg et al, 2007; Ward et al, 1995). A significant proportion of Δ3 GH was detected in the insoluble fraction following MG132 treatment, although the majority of wild-type GH was sorted into the soluble fraction (Fig EV2B). These data suggest that ER-localized Δ3 GH is degraded by the proteasome, leading to Δ3 GH aggregation, which overwhelms the degradative capacity in the cytosol, and that most wild-type GH is not involved in the aggregates.

Δ3 GH-mediated ER stress is not a direct cause of the growth failure of *Gh*$^{wtGH1/\Delta3GH1}$ mice

The enlargement of the rough ER and Δ3 GH aggregates in the cytosol suggest that the *Gh*$^{wtGH1/\Delta3GH1}$ somatotrophs are under ER stress, and we have previously shown that Δ3 GH causes ER stress to the somatotroph *in vitro* (Ariyasu et al, 2013). These data led us to investigate Δ3 GH-mediated ER stress *in vivo*. PKR-like endoplasmic reticulum kinase (PERK), activating transcription factor 6 (ATF6), and inositol requirement 1 (IRE1), are well-characterized ER membrane-located proteins which sense ER stress. In the presence of ER stress, PERK is activated by trans-autophosphorylation, ATF6 activates expression of the ER chaperone immunoglobulin heavy-chain binding protein (BiP), and IRE1 activates splicing of X-box binding protein 1 (*Xbp1*) mRNA via the PERK, ATF6, and IRE1 pathways, respectively (Ariyasu et al, 2017; Yoshida, 2007). PERK phosphorylation can be detected by immunoblotting, as phosphorylated PERK is associated with a mobility shift during SDS-PAGE (Harding et al, 1999). Immunoblotting revealed that the PERK was phosphorylated in 2 and 4-week-old *Gh*$^{wtGH1/\Delta3GH1}$ pituitary glands (Fig 4A). Further, qRT-PCR demonstrated a significant increase in *BiP* mRNA abundance in 4-week-old *Gh*$^{wtGH1/\Delta3GH1}$ pituitary (Fig 4B). *Xbp1* mRNA splicing was evaluated by competitive RT-PCR, using primers flanking the 26 bp sequence spliced out by IRE1α (Yoshida et al, 2001). *Xbp1* mRNA splicing was significantly increased at 1, 2, and 4 weeks of age in *Gh*$^{wtGH1/\Delta3GH1}$ pituitaries (Fig 4C and D).

These data suggest that Δ3 GH can activate the three major ER stress pathways *in vivo*; however, activation of these ER stress pathways is not sufficiently strong to cause somatotroph apoptosis, since no apoptotic cells were detected by TUNEL assay, as described above (Fig 3B), and no caspase-3 activation was detected in *Gh*$^{wtGH1/\Delta3GH1}$ pituitary glands by immunoblotting (Fig 4A). In other established ER stress-related

endocrine diseases, apoptosis is required to cause organ dysfunction (Ariyasu et al, 2017; Fonseca et al, 2010; Hayashi et al, 2009; Oyadomari et al, 2002; Yoshida, 2007). These data suggest that Δ3 GH-mediated ER stress is not likely to be causally related to the growth retardation in *Gh*$^{wtGH1/\Delta3GH1}$ mice.

Decreased *Ghrhr* gene promoter activity contributes to decreased *wtGH1* gene expression in *Gh*$^{wtGH1/\Delta3GH1}$ mice

Our data (described above) indicate that Δ3 GH itself can decrease *wtGH1* mRNA levels, without interacting with wild-type GH protein, ER stress, or apoptosis. RT-PCR revealed that both *wtGH1* and *Δ3GH1* mRNA were equally decreased in *Gh*$^{wtGH1/\Delta3GH1}$ pituitary (Fig 2D), leading us to evaluate the expression levels of genes contributing to upstream regulation of *GH1* gene transcription.

As *wtGH1* mRNA was primarily decreased in *Gh*$^{wtGH1/\Delta3GH1}$ somatotroph, we would expect the *Ghrhr* gene to be overexpressed, because of negative feedback mechanisms reflecting the GH deficiency in this tissue. Consistent with this hypothesis, 4-week-old *Gh*$^{-/-}$ mice had significantly increased abundance of *Ghrhr* mRNA compared with *Gh*$^{wtGH1/wtGH1}$ mice, because of a negative feedback mechanism, reflecting their complete GH deficiency (Fig 5A lane 1 and 3, and B). However, *Gh*$^{wtGH1/\Delta3GH1}$ mice demonstrated significantly decreased *Ghrhr* mRNA compared with *Gh*$^{wtGH1/wtGH1}$ mice, despite their marked GH deficiency (Fig 5A lane 1 and 2, and B). These data suggest that the decrease in *wtGH1* mRNA in *Gh*$^{wtGH1/\Delta3GH1}$ pituitary is mediated, at least in part, by that of *Ghrhr* mRNA. In agreement with this hypothesis, *Gh*$^{\Delta3GH1/-}$ mice demonstrated significantly decreased abundance of *Ghrhr* mRNA, compared with *Gh*$^{-/-}$ mice, despite the fact that both strains lack the ability to secrete wild-type GH (Fig 5A lane 3 and 4, and B). Note that *Gh*$^{\Delta3GH1/-}$ mice demonstrate exactly the same degree of growth retardation as *Gh*$^{-/-}$ mice, because Δ3 GH is not secreted (Fig 5C and EV2C). Further, the decrease in both the abundance of *wtGH1* mRNA in each somatotroph and the number of somatotrophs in *Gh*$^{wtGH1/\Delta3GH1}$ pituitaries (Fig 2G), can be explained by this decrease in *Ghrhr* mRNA, because GHRH signaling is essential for *GH1* gene transcription and somatotroph proliferation (Lin et al, 1993). Taken together, Δ3 GH contributes to decreased *Ghrhr* mRNA levels, without the assistance of wild-type GH, leading to the impaired GHRH signaling and reduced *wtGH1* transcription in *Gh*$^{wtGH1/\Delta3GH1}$ somatotroph.

To evaluate the mechanisms underlying decreases in *Ghrhr* mRNA, a mouse model with the *LacZ* gene knocked in to the *Ghrhr* gene locus (*Ghrhr*$^{+/LacZ}$) was established using the CRISPR/Cas9 gene editing system (Fig EV3A and B). E19.5 and

4-week-old *Ghrhr*$^{+/LacZ}$;*Gh*$^{wtGH1/\Delta3GH1}$ pituitary showed significantly decreased X-gal staining compared with *Ghrhr*$^{+/LacZ}$;*Gh*$^{wtGH1/wtGH1}$ pituitary, indicating that the decreased *Ghrhr* mRNA levels are caused by a reduction in *Ghrhr* promoter activity (Fig 5D).

Nuclear expressions of CREB3L2 is decreased in *Gh*$^{wtGH1/\Delta3GH1}$ pituitary glands

The decreased *Ghrhr* promoter activity detected in *Gh*$^{wtGH1/\Delta3GH1}$ mice suggests that the expression of nuclear transcription factors crucial for the *Ghrhr* expression is disturbed by ER-localized Δ3 GH (Fig 5D). Furthermore, the abnormal cellular organelles and mildly activated ER stress pathway caused by Δ3 GH, indicate that Δ3 GH causes a deterioration in ER function by inducing ER stress (Fig 3C–E, Fig 4A–D). Immunoblotting revealed that abundance of the nuclear POU1F1 protein, a well-known transcription factor involved in regulation of *Ghrhr* and *Gh* promoter activities, was comparable in 4-week-old *Gh*$^{wtGH1/wtGH1}$ and *Gh*$^{wtGH1/\Delta3GH1}$ pituitaries (Fig EV3C), suggesting that other, unknown, pituitary transcription factors were involved in the decreased *Ghrhr* promoter activity in *Gh*$^{wtGH1/\Delta3GH1}$ mice. These data led us to focus on the Creb3 family of bZip transcription factors, a recently described family of ER stress transducers, all of which are ER-bound factors that undergo proteolysis in the Golgi apparatus, leading to production of active N-terminal fragments, which translocate to the nucleus and activate transcription of target genes (Kondo et al, 2011). Five Creb3 family members, CREB3/LUMAN, CREB3L1/OASIS, CREB3L2/BBF2H7, CREB3L3/CREBH, and CREB3L4/TISP40, have been identified to date (DenBoer et al, 2005; Kondo et al, 2005; Kondo et al, 2007; Nagamori et al, 2005; Omori et al, 2001).

Of these, CREB3L1 and CREB3L2 are essential for the differentiation and proliferation of osteoblasts and chondrocytes, respectively. Active N-terminal fragments of CREB3L1 and CREB3L2 bind to cAMP response element (CRE)-like sequences in the promoter regions of target genes, and enhance their expression in osteoblasts and chondrocytes, respectively (Murakami et al, 2009; Saito et al, 2009). Interestingly, *Creb3l1* KO mice display mild growth failure, which is not rescued by osteoblast-specific *Creb3l1* overexpression, but can be ameliorated by exogenous GH treatment, suggesting that they have impaired GH secretion (Murakami et al, 2011). Furthermore, TEM images of *Creb3l1*-deficient osteoblasts and *Creb3l2*-deficient chondrocytes showed abnormal enlarged ER (Murakami et al, 2009; Saito et al, 2009), similar to those detected in *Gh*$^{wtGH1/\Delta3GH1}$ somatotroph. These similarities between *Gh*$^{wtGH1/\Delta3GH1}$ and Creb3 family KO mice led us to hypothesize that one or more Creb3 family members are crucial for *Ghrhr* gene expression, and that the growth failure of *Gh*$^{wtGH1/\Delta3GH1}$ mice is mediated by decreased levels of nuclear active N-terminal Creb3

protein fragments.

RT-PCR analysis of pituitary glands from 4-week-old C57BL/6 mice revealed that the *Creb3l1* and *Creb3l2* genes were strongly expressed in this tissue (Fig 6A). Next, we evaluated expression of these two genes in 4-week-old $Gh^{wtGH1/wtGH1}$ and $Gh^{wtGH1/\Delta3GH1}$ pituitaries by qRT-PCR and immunoblotting. In $Gh^{wtGH1/\Delta3GH1}$ pituitary, the abundance of *Creb3l1* mRNA was increased, while that of the N-terminal CREB3L1 protein was comparable with levels in the $Gh^{wtGH1/wtGH1}$ pituitary (Fig 6B and C). Furthermore, in $Gh^{wtGH1/\Delta3GH1}$ pituitary, *Creb3l2* mRNA levels were comparable, while those of N-terminal CREB3L2 protein were reduced, compared with $Gh^{wtGH1/wtGH1}$ pituitary (Fig 6B and C). Both CREB3L1 and CREB3L2 were demonstrated to be expressed in somatotroph by immunofluorescence (Fig EV3D). These data indicate that expression levels of N-terminal CREB3L1 and CREB3L2 proteins are disturbed in $Gh^{wtGH1/\Delta3GH1}$ mice.

Since involvement of N-terminal CREB3L1 and CREB3L2 in GH production has not been described previously, we evaluated the impact of N-terminal CREB3L1 and CREB3L2 on *Ghrhr* and the *Gh* promoter activities *in vitro*. Luciferase assays revealed that N-terminal CREB3L2 strongly stimulated transcription from both the *Ghrhr* and *Gh* promoters, in combination with POU1F1 (Fig 6D). Decreased nuclear CREB3L2 levels were also demonstrated at embryonic stages in $Gh^{wtGH1/\Delta3GH1}$ pituitary glands by immunoblotting. Ratios of N-terminal CREB3L2 to full-length CREB3L2 decreased in $Gh^{wtGH1/\Delta3GH1}$ pituitary glands at embryonic day E19.5 (Fig 6E and F), indicating that translocation of CREB3L2 to the nucleus was disturbed by ER-localized Δ3 GH. *Sec23a* mRNA, an established target gene of nuclear CREB3L2, was also decreased in $Gh^{wtGH1/\Delta3GH1}$ pituitary at E19.5 (Fig 6G). These data suggest that CREB3L2 stimulates *Ghrhr* and the *Gh* gene expression levels, and that impaired GH production in $Gh^{wtGH1/\Delta3GH1}$ somatotroph is mediated by a decrease in nuclear CREB3L2 levels.

Discussion

The gene exchange system used in this study is a useful method for establishing mouse models of human diseases, because once researchers obtain a gene of interest flanked by mutated *lox* sites, they can easily exchange the endogenous genes with various human genes, via Cre-mediated integration. Using this system, we established a mouse model that expresses the *wtGH1* and *Δ3GH1* genes, instead of endogenous mouse *Gh*. $Gh^{wtGH1/\Delta3GH1}$ mice have two advantages: 1) endogenous mouse GH is not produced and 2) one copy each of human wild-type GH and Δ3 GH are expressed

385 under the control of the *Gh* promoter. Thus, $Gh^{wtGH1/\Delta 3GH1}$ mice are a genetically ideal
386 model that mimics the growth patterns of human patients with IGHD2.
387 For functional analysis of secretory molecules regulated by feedback mechanisms
388 involving in multiple tissues, such as GH, it is important to establish an applicable model
389 that replicates the human disease as precisely as possible. Since patients with IGHD2
390 were first described in 1994, many researchers have focused on interference of
391 wild-type GH protein trafficking by Δ3 GH, and several *in vitro* studies have been
392 conducted to investigate the dominant negative effect of Δ3 GH (Ariyasu et al, 2013;
393 Graves et al, 2001; Hayashi et al, 1999; Iliev et al, 2005; Kannenberg et al, 2007; Lee et
394 al, 2000; McGuinness et al, 2003; Salemi et al, 2006; Salemi et al, 2007); however, in
395 these studies, wild-type and Δ3 GH expression were driven by homeostatic promoters,
396 such as the CMV promoter, and were thus independent of the feedback mechanisms
397 that regulate GH expression *in vivo*. Furthermore, pituitary-derived cell lines, such as
398 GC, GH3, GH4C1, and AtT-20, used in these studies do not express GHRHR. Thus,
399 previous *in vitro* studies have been limited by the absence of feedback mechanisms
400 mimicking those present *in vivo*.
401 The Δ3 GH transgenic mice reported by McGuinness demonstrated massive
402 pituitary damage (McGuinness et al, 2003); however, our $Gh^{wtGH1/\Delta 3GH1}$ mice did not
403 show similar somatotroph loss. The pituitary damage in the Δ3 GH transgenic mice is
404 likely caused by overexpression of the transgene, compared with endogenous mouse
405 *Gh*, since our data indicate that Δ3 GH caused GH deficiency, under conditions of
406 comparable transcriptional efficiency between the mouse *Gh* and *Δ3GH1* alleles (Fig
407 EV1E and F). Further, a previous study using cultured lymphocytes from patients with
408 IGHD2 revealed that ratios of mutant to wild-type *GH1* transcripts were correlated with
409 the severity of GH deficiency (Hamid et al, 2009).
410 In this study, we reveal two important findings: 1) Impaired GH secretion in
411 $Gh^{wtGH1/\Delta 3GH1}$ mice is caused by decreased activity of the *Ghrhr* and *Gh* promoters; 2)
412 these decreases in promoter activity are mediated by reduced levels of nuclear
413 CREB3L2. A schematic representation of the molecular mechanisms underlying GH
414 deficiency in IGHD2 is presented in Fig 7. Our data, including the abnormal TEM
415 images and activated ER stress responses in $Gh^{wtGH1/\Delta 3GH1}$ pituitary, indicate that
416 ER-localized Δ3 GH diminishes ER function by invoking ER stress. Δ3 GH-mediated ER
417 stress leads to a decrease in COPII vesicles, which are essential for ER-Golgi transport,
418 because Δ3 GH disturbs ER-Golgi transport (Graves et al, 2001) and COPII vesicles
419 can be reduced under ER stress conditions (Shaheen, 2018). Full-length CREB3L2 is
420 transported to the Golgi, where it is cleaved to produce the active N-terminal

transcription factor (Kondo et al, 2011); thus a decrease in ER-Golgi transport is expected to reduce nuclear N-terminal CREB3L2 levels, leading to downregulation of both *Ghrhr* and *GH1* gene transcription. The decreased levels of N-terminal CREB3L2 disturb ER-Golgi transport in vicious cycle, since *Sec23a*, an established target gene of N-terminal CREB3L2, encodes SEC23, which is a COPII vesicle coat protein (Saito et al, 2009). Decreased ER-Golgi transport will also influence intracellular protein trafficking of wild-type GH and GHRHR, exacerbating the impaired secretion of wild-type GH. Furthermore, decreased GHRH signaling contributes to GH deficiency through inhibition of somatotroph proliferation. In contrast, decreased *Δ3GH1* gene transcription limits the accumulation of Δ3 GH in the ER, which likely protects the somatotroph from massive ER stress and apoptosis (Fig 7). To our knowledge, this is the first *in vivo* study that has come close to determining the molecular mechanisms underlying GH deficiency in IGHD2.

The involvement of other transcriptions factors, such as CREB3L1 and/or unknown molecules, in the reduction of *Ghrhr* and *Gh* promoter activities is possible. Creb3 members can interact with other bZip transcription factors as heterodimers, to coordinately stimulate transcription of target genes (Saito et al, 2012; Vecchi et al, 2009; Zhang et al, 2006). Hence, identifying the partner molecule of CREB3L2 will be necessary for complete elucidation of the molecular mechanisms involved in IGHD2 GH deficiency.

We presume that CREB3L2 has an important role in the differentiation and proliferation of somatotroph at the late embryonic stage, by stimulating *GHRHR* and *GH1* gene transcription and increasing their secretion, similar to its role in chondrocytes. Postnatal growth has not been described in *Creb3l2*-deficient mice because systemic *Creb3l2* KO mice are lethal soon after birth (Saito et al, 2009). Thus, establishment of somatotroph-specific *Creb3l2* conditional KO mice, and/or $Gh^{wtGH1/\Delta 3GH1}$ mice overexpressing *Creb3l2* specifically in the somatotroph, would be warranted in the future.

Interestingly, exon 3 of the *GH1* gene has weak splice sites, and a small amount of Δ3 GH is produced in the pituitary glands, even in healthy individuals (Lecomte et al, 1987; Ryther et al, 2004). Δ3 GH may have a physiological role in preventing hyperproliferation of somatotroph and overexpression of the *GH1* gene, through the CREB3L2-mediated inhibition of *GHRHR* and *GH1* transcription.

This study has some limitations: 1) it remains unclear whether decreased activity of the *Ghrhr* and *Gh* promoters contributes to the GH deficiency in human IGHD2 patients, because patient pituitary samples are not available. Establishment of

somatotrophs using induced pluripotent stem (iPS) cells derived from IGHD2 patients will help address this issue. 2) The observed decreases in transcriptional activity could be attributed to the influence of the gene exchange process (described in Fig EV1F) on amount of Δ3 GH protein produced, and the cellular characteristics of somatotrophs.

In this study, CREB3L1 and CREB3L2 were demonstrated to be involved in GH production in somatotrophs. These findings suggest that patients with GH deficiency may have mutations in the *Creb3l1* or *Creb3l2* genes, or their binding sites in the *Ghrhr* and *Gh* promoters.

In conclusion, IGHD2 model mice, created using our gene exchange system, reveal a novel molecular mechanism underlying GH deficiency, where ER-localized Δ3 GH leads to decreased levels of nuclear CREB3L2, and a consequent reduction in the activities of the *Ghrhr* and *Gh* promoters.

Materials and Methods

Isolation of the *wtGH1* and *Δ3GH1* genes

The *wtGH1* genomic sequence was amplified from healthy human control lymphocyte DNA using standard PCR methods with a sense primer (GH1-gf1) in the 5′-untranslated region (UTR) and an antisense primer (GH1-gr1) including the termination codon. The *Δ3GH1* genomic sequence, which contains a c.291+1 g>a mutation, was created by mutagenesis, using sense (GH1IVS3-F) and antisense (GH1IVS3dsmut-R) primers containing the single nucleotide substitution. None of the nucleotide polymorphisms, reported to be significantly associated with adult height (Hasegawa et al, 2000) were included in the sequences. All primers used in this study are listed in Supplementary Table 1.

Plasmids

For KO of the *Gh* gene, the 5′ (7 kb) and 3′ (3 kb) arms were isolated by standard PCR methods, using a mouse bacterial artificial chromosome containing the *Gh* gene locus as a template, with sense (Gh-5arm-F and Gh-3arm-F) and antisense (Gh-5arm-R and Gh-3arm-R) primers. These 5′ and 3′ arms were inserted into the gene KO vector (Fig EV1A).

The *wtGH1*, *Δ3GH1*, *Δ3GH1-myc*, or *Gh* gene genomic sequences were inserted to the cassette exchange vector using appropriate restriction enzymes.

To establish the mouse model with *LacZ* knocked-in at the *Ghrhr* gene locus, 5′ (500 bp) and 3′ (450 bp) arms were isolated by standard PCR methods, using sense

(Ghrhr-5arm-f5 and Ghrhr-3arm-f6) and antisense (Ghrhr-5arm-r5 and Ghrhr-3arm-r6) primers, and inserted into a plasmid containing the *LacZ* gene (Fig EV3A).

For CRISPR/Cas9 system plasmids, two pairs of oligonucleotides (Ghrhr-CRI-f1/r1, Ghrhr-CRI-f2/r2, Ghrhr-CRI-f4/r4, Ghrhr-CRI-f5/r5) were annealed and inserted into the pX335-U6-Chimeric_BB-CBh-hSpCas9n(D10A) plasmid (Addgene #42335) (pX335-Ghrhr-1, 2, 4, 5, and pX335-Rosa-3, 4).

For POU1F1, CREB3L1, and CREB3L2 expression plasmids their open reading frames (ORF) were isolated by standard PCR from C57BL/6 pituitary gland template cDNA using sense (Pou1f1-vf1, Creb3l1-vf1, and Creb3l2-vf1) and antisense (Pou1f1-vr1, Creb3l1-vr1, and Creb3l2-vr1) primers, and inserted into the pcDNA4 vector (Invitrogen).

For luciferase assay plasmids, the promoter regions of the *Ghrhr* (500 bp) and *Gh* (400 bp) genes were isolated from C57BL/6 mouse genomic DNA by standard PCR and inserted into the pGL4.10 vector (Promega).

For RNA probes to detect *GH1* and *Ghrhr* mRNAs by *in situ* hybridization, exon 3 of the *GH1* gene (120 bp) and the *Ghrhr* ORF (1272 bp) were amplified by PCR using sense (GH1ex3-f1 and Ghrhr-vf1) and antisense (GH1ex3-r1 and Ghrhr-vr1) primers, with C57BL/6 pituitary gland cDNA as a template, and inserted into the pSP73 vector (Promega).

Embryonic stem cell culture and electroporation

KTPU8 feeder free ES cells, derived from F1 mice obtained by crossing C57BL/6 and CBA strains, were seeded into dishes pretreated with 0.15% gelatin solution, and cultured in Glasgow minimum essential medium, 14% knockout serum replacement, and 100 IU/ml leukemia inhibitory factor. To establish $Gh^{+/-}$ ES cells, KTPU8 cells cultured in a 10 cm culture dish were electroporated (0.8 kV/3 μF) with 20 μg linearized KO vector containing a neomycin resistance (*neoR*) gene flanked by the 5′ and 3′ arms, and seeded into four 10 cm culture dishes. Culture medium containing 180 μg/mL neomycin was exchanged daily. Nine days after electroporation, the surviving clones were picked and DNA from each clone was evaluated by Southern blotting (Fig EV1A and B).

To exchange the *neoR* gene for human *GH1* genes, the $Gh^{+/-}$ ES clones cultured in one 10 cm culture dish were electroporated (0.4 kV/125 μF) with 20 μg exchangeable vector and 10 μg Cre expression vector. Culture medium containing 0.8 μg/mL puromycin was exchanged daily, and the DNA samples of surviving clones were evaluated by Southern blotting (Fig EV1A and B).

To establish a mouse model in which the *LacZ* gene was knocked-in at the *Ghrhr* gene locus, ES cells derived from C57BL/6 mice were electroporated (0.4 kV/125 μF) with 25 μg plasmid containing the *LacZ* gene flanked by *Ghrhr* homology arms, pX335-Ghrhr-1 and pX335-Ghrhr-2 (15 μg each) (Fig EV3A). For this process, we took advantage of D10A mutant Cas9, to avoid making double-strand breaks (Cong et al, 2013; Jinek et al, 2012).

Southern Blotting

Southern blotting was conducted using DIG, according to the manufacturer's protocol. For *Gh* gene knockout, homologous recombination of the *neoR* gene was confirmed by Southern blotting using probes for sequences flanking the 5′ and 3′ arms, and the *neoR* gene (Fig EV1A and B). Substitution of the *GH1* gene for *neoR* was also evaluated by Southern blotting, using probes for the puromycin resistance gene (*PuroR*) (Fig EV1B). To evaluate knock-in of the *LacZ* gene at the *Ghrhr* gene locus, Southern blotting was performed, using probes for sequences flanking the 5′ and 3′ arms (Fig EV3A and B).

RT-PCR and quantitative RT-PCR (qRT-PCR)

Total RNA was extracted from mouse pituitaries using an RNeasy mini kit (Qiagen) and 250 ng converted to cDNA using Revertra Ace (TOYOBO, Osaka, Japan, FSQ-101). cDNA aliquots were used for RT-PCR and qRT-PCR.

For qRT-PCR, THUNDERBIRD SYBR qPCR Mix (TOYOBO, QPS-201) was used as Taq polymerase and reactions were performed using the SYBR method on an Applied Biosystems 7500 Real-Time PCR System (Applied Biosystems, Foster City, CA). In experiments using relative quantification, the relative concentrations of target mRNAs were calculated using a standard curve and normalized to *β*-actin expression.

SDS-PAGE and immunoblotting

SDS-PAGE and immunoblotting were carried out using polyacrylamide gels, polyvinylidene difluoride membranes, and ECL select detection reagent (Amersham, Buckinghamshire, England, RPN2235) according to standard procedures (Sambrook et al).

Antibodies

For immunoblotting assays, the following primary antibodies were used: 1) anti-GH rabbit polyclonal antibody (Dako, A0570) (dilution 1:3000); 2) anti-PERK rabbit

monoclonal antibody C33E10 (Cell Signaling Technology, 3192) (dilution 1:1000); 3) anti-caspase-3 rabbit monoclonal antibody 8G10 (Cell Signaling Technology, 9665) (dilution 1:1000); 4) anti-GRP78 rabbit monoclonal antibody EPR4041(2) (Abcam, ab108615) (dilution 1:500); 5) anti-GAPDH mouse monoclonal antibody 6C5 (Santa Cruz, sc-32233) (dilution 1:5000); 6) anti-LAMIN A/C rabbit polyclonal antibody (Cell Signaling Technology, 2032) (dilution 1:1000); 7) anti-POU1F1 mouse monoclonal antibody 2C11 (Abcam, ab10623) (dilution 1:1000); 8) anti-CREB3L1 mouse monoclonal antibody 44c7 (Merck Millipore, MABE1017) (dilution 1:1000); 9) anti-CREB3L2 rabbit polyclonal antibody (kindly provided by Prof. Imaizumi, Hiroshima University, Japan) (dilution 1:1000). Anti-rabbit immunoglobulin (IgG) (Dako, P0399) and anti-mouse immunoglobulin (Abcam, ab205719) (dilution 1:5000) secondary antibodies were used.

For immunohistochemistry, the following primary antibodies were used at a 1:100 dilution: 1) anti-GH rabbit polyclonal antibody (Dako, A0570); 2) anti-GH mouse monoclonal antibody (Abcam, ab15317); 3) anti-CREB3L1 rabbit polyclonal antibody (Abcam, ab33051); and 4) anti-CREB3L2 rabbit polyclonal antibody (kindly provided by Prof. Imaizumi). Goat anti-rabbit IgG (Abcam, ab150079, and Dako, P0448) (dilution 1:100) and M.O.M. biotinylated anti-mouse IgG reagent (VECTOR, MKB-2225) secondary antibodies were used. Fluorescein avidin DCS (VECTOR, A-2011) was used with the anti-mouse IgG reagent (MKB-2225).

Luciferase assay

BMT10 cells were seeded into 96-well plates at a density of 5000 cells/well. Next day, plasmids expressing POU1F1, CREB3L1-N, and CREB3L2-N or empty vector were mixed in various combinations and transfected using Lipofectamine 2000 (Invitrogen). Forty-eight hours later, luciferase assay was performed using Dual-Luciferase Reporter Assay System (Promega).

3-D structural analyses of GH proteins

The 3-D structure of wild-type GH was obtained from the Protein Data Bank (PDB ID: 1AXI) and that of Δ3 GH was analyzed using the homology model function of MOE software (Chemical Computing Group Inc.), as described previously (Nakamura et al, 2017; Ogasawara et al, 2016). Hydrogen atoms were then added to each protein, using the protonate 3D function of MOE under ER pH conditions (Kim et al, 1998). These structures were then subjected to molecular mechanics (MM) calculations using MOE, with the AMBER99 force field, until the root mean square gradient was 0.01 kcal/mol/Å.

After heating for 250 ps to attain 310 K as the starting temperature, a 5000 ps production run of the molecular dynamic (MD) simulation was performed at 310 K, with NPT ensemble using NAMD software (Phillips et al, 2005).

Docking simulation analysis of dimeric GH molecules

Docking simulations were performed using ZDOCK (Chen et al, 2003) with residues within 10 Å of cysteine residues (numbers 79, 191, 208, and 215) defined as docking sites in each protein (Ogasawara et al, 2016; Yasui et al, 2013). Two thousand docking runs were performed for each pair of GH molecules and docking poses were classified according to the distance between cysteine residues in the two GHs. The number and binding affinities of docking poses which could form dimers via intermolecular disulfide bonds (Grigorian et al, 2005) were analyzed.

Animals

ICR and C57BL/6 mice were purchased from CLEA Japan, Inc. Egg zona pellucida from E2.5 ICR mouse embryos were removed and aggregated with KTPU8 ES clones. The resulting blastocysts were transferred to the uteruses of ICR female mice mated with vasoligated male mice. F0 mice, with 100% chimerism, were crossed with C57BL/6 mice, to obtain N1 offspring. $Gh^{wtGH1/wtGH1}$ and $Gh^{wtGH1/\Delta 3GH1}$ mice were backcrossed to C57BL/6 mice for at least ten generations.

Genotyping

To determine mouse genotypes, standard PCR reactions were performed using template DNA samples extracted from toe clips from 7-day-old mice (Fig EV1A and D). A reverse primer with the 3′ end converted to thymine from cytosine at the first base of the intron 3 in the *GH1* gene (primer No. 4, completely matching the *Δ3GH1* allele) was used. PCR reactions to detect both *wtGH1* and *Δ3GH1* alleles used an annealing temperature of 60℃, with those to detect only the *Δ3GH1* allele using an annealing temperature of 66℃ (Fig EV1D). The sequences of all primers used in this study are listed in Table 1.

Measurement of mouse body weight and length

Mouse body weights were measured every week from 1 to 16 weeks of age. Body lengths (distances from nose to anus) were measured under anesthesia, induced using isoflurane, every 4 weeks from 4 to 16 weeks of age, using a ruler.

Measurement of mouse serum IGF-1 concentration

Blood samples were obtained from mouse orbital veins at 4 weeks of age, using a heparinized tube. Samples were centrifuged at 3000 rpm for 5 min, to collect serum samples collected. IGF-1 concentrations were evaluated using a Mouse/Rat IGF-1 ELISA Kit (ALPCO, 22-IG1MS-E01).

Hematoxylin and eosin (HE) staining, TUNEL assay, and Immunohistochemistry

Pituitary glands were fixed in 4% paraformaldehyde (PFA) for 24 h at 15-25 ℃, dehydrated through increasing concentrations of ethanol, equilibrated with xylene, embedded in paraffin wax, and sectioned at 4 μm. Pituitary sections were stained with hematoxylin and eosin and examined by light microscopy. TUNEL assays were performed using an ApopTag Peroxidase In Situ Apoptosis Detection Kit (Millipore, S7100). Thymus sections were used as positive controls. For immunostaining of GH, pituitary sections were deparaffinized, rehydrated, and treated with 20 μg/ml proteinase K as an antigen retrieval step. Antibodies are described in the 'antibodies' section above. Staining was performed using diaminobenzidine (DAB) and hematoxylin.

Immunofluorescence assay

Pituitary glands were fixed in 4% PFA for 2 h at room temperature, dehydrated through increasing concentrations of sucrose, embedded in Optimal Cutting Temperature Compound, and sectioned at 6 μm. Frozen pituitary sections were subjected to immunofluorescence analysis.

***In situ* hybridization**

Pituitary glands were fixed in 4% PFA for 48 h at room temperature. Deparaffinization, cell conditioning, prehybridization, and stringency washing were automated using a staining workstation (Ventana Discovery XT). RNA probes were synthesized by *in vitro* transcription, and labelled with digoxigenin (DIG), using a DIG RNA labeling kit (Roche, 11175025910). Probes for *wtGH1* and *Ghrhr* mRNAs were manually hybridized at 0.5 ng/ml, 65℃ for 6 h, and 10 ng/ml, 68℃ for 6 h, respectively.

Transmission electron microscopy

Pituitary glands from four-week-old mice were used for TEM observation, as described previously (Shibata et al, 2015). Briefly, tissues were dissected out and fixed in 2.5% glutaraldehyde in 0.1 M phosphate buffer (pH 7.4) for 24 h at 4°C. After 2 h post-fixation with 1% OsO_4 and dehydration through ethanol, then acetone with n-butyl

673 glycidyl ether (QY1) including a graded concentration of Epon with QY-1, they were
674 embedded into 100% Epon. Following 72 h of polymerization in pure Epon, 70 nm
675 ultrathin coronal pituitary gland sections were prepared on copper grids and stained with
676 uranyl acetate and lead citrate for 10 min. Sections were observed under a TEM (JEOL
677 JEM-1400 plus).
678
679 **X-gal staining of pituitary glands**
680 Pituitary glands were removed from four-week-old mice and fixed in 4% PFA for 1
681 h on ice. Then, samples were permeabilized using rinse buffer (phosphate buffered
682 saline (PBS) containing 2 mM $MgCl_2$, 0.01% sodium deoxycholate, and 0.02% Nonidet
683 P-40) for 2 h on ice, washed three times for 30 min in PBS, and stained in rinse buffer
684 containing 5 mM potassium ferricyanide, 5 mM potassium ferrocyanide, and 1 mg/ml
685 5-Bromo-4-Chloro-3-Indolyl-β-D-Galactoside (X-gal) overnight at 37℃. For E19.5
686 embryo samples, heads were removed and fixed in 4% PFA for 30 min on ice. Then,
687 pituitary glands were exposed by removing the skull bone and brain before
688 permeabilization using rinse buffer.
689
690 **Dissociation of pituitary cells**
691 Anterior pituitary cells were dissociated, according to published methods, using
692 0.5 % trypsin-EDTA (Oomizu et al, 1998).
693
694 **Soluble/insoluble fraction assay, cytoplasmic/nuclear fraction assay**
695 For soluble/insoluble fraction assays, anterior pituitary cells were dissociated as
696 described above, and 0.5 x 10^6 cells seeded in DMEM with 10% FBS in a 24-well plate
697 with 10 μM MG132 (Peptide Institute, Osaka, Japan), or DMSO, for 4 h. Detailed
698 procedures have been described elsewhere (Ariyasu et al, 2013). To separate
699 cytoplasmic and nuclear fractions, a NE-PER Nuclear and Cytoplasmic Reagent Kit
700 (Thermo Fischer Scientific, 78833) was used.
701
702 **Statistics**
703 Data were analyzed by 2-tailed unpaired Student's *t* test for comparisons of two
704 groups. For all bar graphs, means ± SD are plotted.
705
706 **Study approval**
707 The Animal Care Committee and Institutional Biosafety Committee of the
708 Kumamoto University approved all mouse protocols. All experiments were performed in

accordance with the Declaration of Helsinki and were approved by the Kumamoto University Ethics Committee for Animal Experiments (authorization number in Kumamoto University: C23-262, C24-278).

Acknowledgments

This work was supported by JSPS KAKENHI Grant Numbers JP16H06276 and JP16H07081. The authors thank Mayumi Muta, Kumiko Murakami, Mai Nakahara, and Riki Furuhata for assistance with embryo manipulation; Michiyo Nakata and Sayoko Fujimura for assistance with preparing paraffin-embedded and frozen pituitary samples; Hiderou Yoshida for giving important advice regarding ER stress-related experiments; Haruo Nogami for providing information about *Ghrhr* promoter activity; and Yukihiro Hasegawa for fruitful discussions about the manuscript and long-standing support.

Author contributions

DA and KA conceived the study. DA and KA designed the experiments. DA, EK, DH, YT, and SS performed the experiments and analyzed the data. DA, SS, and YT wrote the initial draft of the paper. TH, MS, KI, and KA critically revised the manuscript. All authors reviewed and edited the manuscript.

Conflict of Interest

The authors have declared that no conflict of interest exists.

References

Akinci A, Kanaka C, Eble A, Akar N, Vidinlisan S, Mullis PE (1992) Isolated growth hormone (GH) deficiency type IA associated with a 45-kilobase gene deletion within the human GH gene cluster. *The Journal of clinical endocrinology and metabolism* **75:** 437-441

Araki K, Araki M, Yamamura K (2002) Site-directed integration of the cre gene mediated by Cre recombinase using a combination of mutant lox sites. *Nucleic acids research* **30:** e103

Ariyasu D, Yoshida H, Hasegawa Y (2017) Endoplasmic Reticulum (ER) Stress and Endocrine Disorders. *International journal of molecular sciences* **18**

745 Ariyasu D, Yoshida H, Yamada M, Hasegawa Y (2013) Endoplasmic reticulum stress
746 and apoptosis contribute to the pathogenesis of dominantly inherited isolated GH
747 deficiency due to GH1 gene splice site mutations. *Endocrinology* **154:** 3228-3239
748
749 Binder G, Ranke MB (1995) Screening for growth hormone (GH) gene splice-site
750 mutations in sporadic cases with severe isolated GH deficiency using ectopic transcript
751 analysis. *The Journal of clinical endocrinology and metabolism* **80:** 1247-1252
752
753 Chen R, Li L, Weng Z (2003) ZDOCK: an initial-stage protein-docking algorithm.
754 *Proteins* **52:** 80-87
755
756 Cogan JD, Phillips JA, 3rd, Schenkman SS, Milner RD, Sakati N (1994) Familial growth
757 hormone deficiency: a model of dominant and recessive mutations affecting a
758 monomeric protein. *The Journal of clinical endocrinology and metabolism* **79:**
759 1261-1265
760
761 Cong L, Ran FA, Cox D, Lin S, Barretto R, Habib N, Hsu PD, Wu X, Jiang W, Marraffini
762 LA, Zhang F (2013) Multiplex genome engineering using CRISPR/Cas systems.
763 *Science* **339:** 819-823
764
765 Deladoey J, Stocker P, Mullis PE (2001) Autosomal dominant GH deficiency due to an
766 Arg183His GH-1 gene mutation: clinical and molecular evidence of impaired regulated
767 GH secretion. *The Journal of clinical endocrinology and metabolism* **86:** 3941-3947
768
769 DenBoer LM, Hardy-Smith PW, Hogan MR, Cockram GP, Audas TE, Lu R (2005)
770 Luman is capable of binding and activating transcription from the unfolded protein
771 response element. *Biochemical and biophysical research communications* **331:**
772 113-119
773
774 Fonseca SG, Ishigaki S, Oslowski CM, Lu S, Lipson KL, Ghosh R, Hayashi E, Ishihara
775 H, Oka Y, Permutt MA, Urano F (2010) Wolfram syndrome 1 gene negatively regulates
776 ER stress signaling in rodent and human cells. *The Journal of clinical investigation* **120:**
777 744-755
778
779 Graves TK, Patel S, Dannies PS, Hinkle PM (2001) Misfolded growth hormone causes
780 fragmentation of the Golgi apparatus and disrupts endoplasmic reticulum-to-Golgi traffic.

Journal of cell science **114:** 3685-3694

Grigorian AL, Bustamante JJ, Hernandez P, Martinez AO, Haro LS (2005) Extraordinarily stable disulfide-linked homodimer of human growth hormone. *Protein science : a publication of the Protein Society* **14:** 902-913

Hamid R, Phillips JA, 3rd, Holladay C, Cogan JD, Austin ED, Backeljauw PF, Travers SH, Patton JG (2009) A molecular basis for variation in clinical severity of isolated growth hormone deficiency type II. *The Journal of clinical endocrinology and metabolism* **94:** 4728-4734

Harding HP, Zhang Y, Ron D (1999) Protein translation and folding are coupled by an endoplasmic-reticulum-resident kinase. *Nature* **397:** 271-274

Hasegawa Y, Fujii K, Yamada M, Igarashi Y, Tachibana K, Tanaka T, Onigata K, Nishi Y, Kato S, Hasegawa T (2000) Identification of novel human GH-1 gene polymorphisms that are associated with growth hormone secretion and height. *The Journal of clinical endocrinology and metabolism* **85:** 1290-1295

Hayashi M, Arima H, Ozaki N, Morishita Y, Hiroi M, Nagasaki H, Kinoshita N, Ueda M, Shiota A, Oiso Y (2009) Progressive polyuria without vasopressin neuron loss in a mouse model for familial neurohypophysial diabetes insipidus. *American journal of physiology Regulatory, integrative and comparative physiology* **296:** R1641-1649

Hayashi Y, Yamamoto M, Ohmori S, Kamijo T, Ogawa M, Seo H (1999) Inhibition of growth hormone (GH) secretion by a mutant GH-I gene product in neuroendocrine cells containing secretory granules: an implication for isolated GH deficiency inherited in an autosomal dominant manner. *The Journal of clinical endocrinology and metabolism* **84:** 2134-2139

Iliev DI, Wittekindt NE, Ranke MB, Binder G (2005) Structural analysis of human growth hormone with respect to the dominant expression of growth hormone (GH) mutations in isolated GH deficiency type II. *Endocrinology* **146:** 1411-1417

Imai Y, Soda M, Inoue H, Hattori N, Mizuno Y, Takahashi R (2001) An unfolded putative transmembrane polypeptide, which can lead to endoplasmic reticulum stress, is a

817 substrate of Parkin. *Cell* **105:** 891-902
818
819 Ito M, Yu RN, Jameson JL (1999) Mutant vasopressin precursors that cause autosomal
820 dominant neurohypophyseal diabetes insipidus retain dimerization and impair the
821 secretion of wild-type proteins. *The Journal of biological chemistry* **274:** 9029-9037
822
823 Jacobson EM, Li P, Leon-del-Rio A, Rosenfeld MG, Aggarwal AK (1997) Structure of
824 Pit-1 POU domain bound to DNA as a dimer: unexpected arrangement and flexibility.
825 *Genes Dev* **11:** 198-212
826
827 Jinek M, Chylinski K, Fonfara I, Hauer M, Doudna JA, Charpentier E (2012) A
828 programmable dual-RNA-guided DNA endonuclease in adaptive bacterial immunity.
829 *Science* **337:** 816-821
830
831 Kannenberg K, Wittekindt NE, Tippmann S, Wolburg H, Ranke MB, Binder G (2007)
832 Mutant and misfolded human growth hormone is rapidly degraded through the
833 proteasomal degradation pathway in a cellular model for isolated growth hormone
834 deficiency type II. *Journal of neuroendocrinology* **19:** 882-890
835
836 Kim JH, Johannes L, Goud B, Antony C, Lingwood CA, Daneman R, Grinstein S (1998)
837 Noninvasive measurement of the pH of the endoplasmic reticulum at rest and during
838 calcium release. *Proceedings of the National Academy of Sciences of the United States*
839 *of America* **95:** 2997-3002
840
841 Kondo S, Murakami T, Tatsumi K, Ogata M, Kanemoto S, Otori K, Iseki K, Wanaka A,
842 Imaizumi K (2005) OASIS, a CREB/ATF-family member, modulates UPR signalling in
843 astrocytes. *Nature cell biology* **7:** 186-194
844
845 Kondo S, Saito A, Asada R, Kanemoto S, Imaizumi K (2011) Physiological unfolded
846 protein response regulated by OASIS family members, transmembrane bZIP
847 transcription factors. *IUBMB life* **63:** 233-239
848
849 Kondo S, Saito A, Hino S, Murakami T, Ogata M, Kanemoto S, Nara S, Yamashita A,
850 Yoshinaga K, Hara H, Imaizumi K (2007) BBF2H7, a novel transmembrane bZIP
851 transcription factor, is a new type of endoplasmic reticulum stress transducer. *Molecular*
852 *and cellular biology* **27:** 1716-1729

Lecomte CM, Renard A, Martial JA (1987) A new natural hGH variant--17.5 kd--produced by alternative splicing. An additional consensus sequence which might play a role in branchpoint selection. *Nucleic acids research* **15:** 6331-6348

Lee MS, Wajnrajch MP, Kim SS, Plotnick LP, Wang J, Gertner JM, Leibel RL, Dannies PS (2000) Autosomal dominant growth hormone (GH) deficiency type II: the Del32-71-GH deletion mutant suppresses secretion of wild-type GH. *Endocrinology* **141:** 883-890

Lin SC, Lin CR, Gukovsky I, Lusis AJ, Sawchenko PE, Rosenfeld MG (1993) Molecular basis of the little mouse phenotype and implications for cell type-specific growth. *Nature* **364:** 208-213

Lochmatter D, Strom M, Eble A, Petkovic V, Fluck CE, Bidlingmaier M, Robinson IC, Mullis PE (2010) Isolated GH deficiency type II: knockdown of the harmful Delta3GH recovers wt-GH secretion in rat tumor pituitary cells. *Endocrinology* **151:** 4400-4409

McGuinness L, Magoulas C, Sesay AK, Mathers K, Carmignac D, Manneville JB, Christian H, Phillips JA, 3rd, Robinson IC (2003) Autosomal dominant growth hormone deficiency disrupts secretory vesicles in vitro and in vivo in transgenic mice. *Endocrinology* **144:** 720-731

Miletta MC, Fluck CE, Mullis PE (2017) Targeting GH-1 splicing as a novel pharmacological strategy for growth hormone deficiency type II. *Biochemical pharmacology* **124:** 1-9

Miletta MC, Petkovic V, Eble A, Fluck CE, Mullis PE (2016) Rescue of Isolated GH Deficiency Type II (IGHD II) via Pharmacologic Modulation of GH-1 Splicing. *Endocrinology* **157:** 3972-3982

Mullis PE, Deladoey J, Dannies PS (2002) Molecular and cellular basis of isolated dominant-negative growth hormone deficiency, IGHD type II: insights on the secretory pathway of peptide hormones. *Hormone research* **58:** 53-66

Murakami T, Hino S, Nishimura R, Yoneda T, Wanaka A, Imaizumi K (2011) Distinct

mechanisms are responsible for osteopenia and growth retardation in OASIS-deficient mice. *Bone* **48:** 514-523

Murakami T, Saito A, Hino S, Kondo S, Kanemoto S, Chihara K, Sekiya H, Tsumagari K, Ochiai K, Yoshinaga K, Saitoh M, Nishimura R, Yoneda T, Kou I, Furuichi T, Ikegawa S, Ikawa M, Okabe M, Wanaka A, Imaizumi K (2009) Signalling mediated by the endoplasmic reticulum stress transducer OASIS is involved in bone formation. *Nature cell biology* **11:** 1205-1211

Nagamori I, Yabuta N, Fujii T, Tanaka H, Yomogida K, Nishimune Y, Nojima H (2005) Tisp40, a spermatid specific bZip transcription factor, functions by binding to the unfolded protein response element via the Rip pathway. *Genes to cells : devoted to molecular & cellular mechanisms* **10:** 575-594

Nakamura Y, Sugano A, Ohta M, Takaoka Y (2017) Docking analysis and the possibility of prediction efficacy for an anti-IL-13 biopharmaceutical treatment with tralokinumab and lebrikizumab for bronchial asthma. *PloS one* **12:** e0188407

Ogasawara M, Nakamura Y, Morikawa N, Nitanai H, Moriguchi S, Chiba R, Saito H, Ohta M, Tanita T, Sugai T, Maeyama K, Yamauchi K, Takaoka Y (2016) Analysis of a single-codon E746 deletion in exon 19 of the epidermal growth factor receptor. *Cancer chemotherapy and pharmacology* **77:** 1019-1029

Omori Y, Imai J, Watanabe M, Komatsu T, Suzuki Y, Kataoka K, Watanabe S, Tanigami A, Sugano S (2001) CREB-H: a novel mammalian transcription factor belonging to the CREB/ATF family and functioning via the box-B element with a liver-specific expression. *Nucleic acids research* **29:** 2154-2162

Oomizu S, Takeuchi S, Takahashi S (1998) Stimulatory effect of insulin-like growth factor I on proliferation of mouse pituitary cells in serum-free culture. *The Journal of endocrinology* **157:** 53-62

Oyadomari S, Koizumi A, Takeda K, Gotoh T, Akira S, Araki E, Mori M (2002) Targeted disruption of the Chop gene delays endoplasmic reticulum stress-mediated diabetes. *The Journal of clinical investigation* **109:** 525-532

925 Petkovic V, Godi M, Lochmatter D, Eble A, Fluck CE, Robinson IC, Mullis PE (2010)
926 Growth hormone (GH)-releasing hormone increases the expression of the
927 dominant-negative GH isoform in cases of isolated GH deficiency due to GH splice-site
928 mutations. *Endocrinology* **151:** 2650-2658
929
930 Phillips JC, Braun R, Wang W, Gumbart J, Tajkhorshid E, Villa E, Chipot C, Skeel RD,
931 Kale L, Schulten K (2005) Scalable molecular dynamics with NAMD. *Journal of*
932 *computational chemistry* **26:** 1781-1802
933
934 Ryther RC, Flynt AS, Harris BD, Phillips JA, 3rd, Patton JG (2004) GH1 splicing is
935 regulated by multiple enhancers whose mutation produces a dominant-negative GH
936 isoform that can be degraded by allele-specific small interfering RNA (siRNA).
937 *Endocrinology* **145:** 2988-2996
938
939 Saito A, Hino S, Murakami T, Kanemoto S, Kondo S, Saitoh M, Nishimura R, Yoneda T,
940 Furuichi T, Ikegawa S, Ikawa M, Okabe M, Imaizumi K (2009) Regulation of
941 endoplasmic reticulum stress response by a BBF2H7-mediated Sec23a pathway is
942 essential for chondrogenesis. *Nature cell biology* **11:** 1197-1204
943
944 Saito A, Kanemoto S, Kawasaki N, Asada R, Iwamoto H, Oki M, Miyagi H, Izumi S,
945 Sanosaka T, Nakashima K, Imaizumi K (2012) Unfolded protein response, activated by
946 OASIS family transcription factors, promotes astrocyte differentiation. *Nature*
947 *communications* **3:** 967
948
949 Salemi S, Yousefi S, Eble A, Deladoey J, Mullis PE (2006) Impact of del32-71-GH (exon
950 3 skipped GH) on intracellular GH distribution, secretion and cell viability: a quantitative
951 confocal microscopy analysis. *Hormone research* **65:** 132-141
952
953 Salemi S, Yousefi S, Lochmatter D, Eble A, Deladoey J, Robinson IC, Simon HU, Mullis
954 PE (2007) Isolated autosomal dominant growth hormone deficiency: stimulating mutant
955 GH-1 gene expression drives GH-1 splice-site selection, cell proliferation, and apoptosis.
956 *Endocrinology* **148:** 45-53
957
958 Sambrook J, Eritsch E, Maniatis T *Molecular Cloning: A Laboratory Manual*, New
959 York: Cold Spring Harbor Laboratory Press.
960

961 Shaheen A (2018) Effect of the unfolded protein response on ER protein export: a
962 potential new mechanism to relieve ER stress. *Cell stress & chaperones* **23:** 797-806
963
964 Shibata S, Murota Y, Nishimoto Y, Yoshimura M, Nagai T, Okano H, Siomi MC (2015)
965 Immuno-Electron Microscopy and Electron Microscopic In Situ Hybridization for
966 Visualizing piRNA Biogenesis Bodies in Drosophila Ovaries. *Methods Mol Biol* **1328:**
967 163-178
968
969 Vecchi C, Montosi G, Zhang K, Lamberti I, Duncan SA, Kaufman RJ, Pietrangelo A
970 (2009) ER stress controls iron metabolism through induction of hepcidin. *Science* **325:**
971 877-880
972
973 Ward CL, Omura S, Kopito RR (1995) Degradation of CFTR by the
974 ubiquitin-proteasome pathway. *Cell* **83:** 121-127
975
976 Yasui N, Takaoka Y, Nishio H, Nurputra DK, Sekiguchi K, Hamaguchi H, Kowa H,
977 Maeda E, Sugano A, Miura K, Sakaeda T, Kanda F, Toda T (2013) Molecular pathology
978 of Sandhoff disease with p.Arg505Gln in HEXB: application of simulation analysis.
979 *Journal of human genetics* **58:** 611-617
980
981 Yoshida H (2007) ER stress and diseases. *The FEBS journal* **274:** 630-658
982
983 Yoshida H, Matsui T, Yamamoto A, Okada T, Mori K (2001) XBP1 mRNA is induced by
984 ATF6 and spliced by IRE1 in response to ER stress to produce a highly active
985 transcription factor. *Cell* **107:** 881-891
986
987 Zhang K, Shen X, Wu J, Sakaki K, Saunders T, Rutkowski DT, Back SH, Kaufman RJ
988 (2006) Endoplasmic reticulum stress activates cleavage of CREBH to induce a systemic
989 inflammatory response. *Cell* **124:** 587-599
990

991 ## Figure Legends

992

993 Figure 1

994 *Gh*$^{wtGH1/\Delta 3GH1}$ mice exhibit a Δ3 GH-mediated dominant negative phenotype.

995 (A) Schematic representations of wild-type and genetically modified alleles. Vertical
996 long open and closed rectangles represent the 5 exons of the endogenous *Gh* gene and

997 the exchanged human *GH1* gene, respectively. Orange and purple rectangles,
998 untranslated regions of the *Gh* gene. Red closed circle, c.291+1 g>a mutation. hACp,
999 human actin promoter; neoR, neomycin resistance gene; pPGK, phosphoglycerate
1000 kinase promoter; PuroR, puromycin resistance gene; pA, polyadenylation signal.
1001 (B, C) Growth curves of model mice. (B) Body weight (BW) and (C) body length (BL)
1002 were measured every week and every 4 weeks, respectively, up to 16 weeks of age.
1003 Asterisks indicate that data from $Gh^{wtGH1/\Delta 3GH1}$ mice are significantly different to those
1004 from $Gh^{wtGH1/wtGH1}$ mice. Means calculated from the indicated numbers of model mice
1005 (bottom right in (B)) are shown. Error bars represent the standard deviation (SD) of
1006 values in $Gh^{wtGH1/wtGH1}$ and $Gh^{wtGH1/\Delta 3GH1}$ mice. *p<0.01, **p<0.005.
1007 (D) Serum IGF-1 values in 4-week-old model mice. Mean and SD values from six mice
1008 with each genotype are shown. **p<0.005.
1009 (E) Photograph of male $Gh^{wtGH1/wtGH1}$, $Gh^{wtGH1/-}$, $Gh^{wtGH1/\Delta 3GH1}$, and $Gh^{-/-}$ mice at 8 weeks
1010 old.
1011
1012 Figure 2
1013 Evaluation of wild-type and Δ3 GH expression in $Gh^{wtGH1/wtGH1}$ and $Gh^{wtGH1/\Delta 3GH1}$ pituitary
1014 samples.
1015 (A) Immunoblotting using anti-GH antibody. This antibody recognizes Δ3 GH; however,
1016 the 17.5 kDa signals were too faint to be detected in $Gh^{wtGH1/\Delta 3GH1}$ pituitary glands. An
1017 image obtained by long exposure is shown on the right.
1018 (B) Evaluation of wild-type GH expression in (A) by densitometry. *p<0.05.
1019 (C) Results of immunohistochemistry using the same antibody used in (A). Scale bars,
1020 100 μM.
1021 (D) Abundance of *wtGH1* and *Δ3GH1* mRNAs, evaluated by RT-PCR using a sense
1022 primer in exon 1 and an antisense primer in exon 5.
1023 (E) Evaluation of *wtGH1* mRNA abundance by qRT-PCR, using a sense primer in exon
1024 3 and an antisense primer spanning exons 3 and 4. Data presented are mean and SD
1025 values from three independent samples, with relative abundance calculated by
1026 normalization to *β-actin* expression. ***p<0.005.
1027 (F) Results of qRT-PCR to evaluate the abundance of *wtGH1* mRNA using pituitary
1028 samples from $Gh^{wtGH1/wtGH1}$ and $Gh^{wtGH1/\Delta 3GH1}$ mice at E19.5, and 1, 2, 3, and 4 weeks of
1029 age. **p<0.01, ***p<0.005.
1030 (G) *In situ* hybridization of pituitary gland samples from E19.5 and 4-week-old mice,
1031 using an antisense probe complementary to *GH1* exon 3 mRNA. Scale bars, 100 μM.
1032

Figure 3

Histological evaluation of pituitary glands from *Gh*$^{wtGH1/wtGH1}$ and *Gh*$^{wtGH1/Δ3GH1}$ mice.

(A) Stereomicroscope images of pituitary glands from 4-week-old *Gh*$^{+/+}$, *Gh*$^{wtGH1/wtGH1}$, *Gh*$^{wtGH1/-}$, *Gh*$^{wtGH1/Δ3GH1}$, and *Gh*$^{-/-}$ mice. Scale bars, 2 mm.

(B) HE (scale bars, 50 μM) and TUNEL staining (scale bars, 100 μM) of pituitary glands from 4-week-old *Gh*$^{wtGH1/wtGH1}$ and *Gh*$^{wtGH1/Δ3GH1}$ mice.

(C, D) TEM images of pituitary glands from 4-week-old (C) *Gh*$^{wtGH1/wtGH1}$ and *Gh*$^{wtGH1/Δ3GH1}$, and (D) *Gh*$^{-/-}$ and *Gh*$^{Δ3GH1/-}$, mice. Marked enlargement of the rough ER (arrow) and cytosolic protein aggregates (arrowhead) were observed in *Gh*$^{wtGH1/Δ3GH1}$ and *Gh*$^{Δ3GH1/-}$ somatotroph. Scale bars, 10 μM (low power field) and 2 μM (high power field).

(E) Magnified view of the open square in (C). The rough ER membrane is connected to the protein aggregates (arrowhead). Scale bar, 1 μM.

(F) Evaluation of cellular localization of Δ3GH-myc by immunofluorescence, using antibodies against the myc-tag (Δ3GH-myc), KDEL (ER marker), and GM130 (Golgi marker).

Figure 4

Δ3 GH activates three major ER stress response pathways.

(A) Evaluation of phosphorylation of PERK, expression of BiP, and activation of caspase-3 by immunoblotting using pituitary glands from 2 and 4-week-old *Gh*$^{wtGH1/wtGH1}$ and *Gh*$^{wtGH1/Δ3GH1}$ mice.

(B) qRT-PCR evaluation of the abundance of *BiP* mRNA in pituitary glands from 2 and 4-week-old *Gh*$^{wtGH1/wtGH1}$ and *Gh*$^{wtGH1/Δ3GH1}$ mice. **p<0.01.

(C) RT-PCR evaluation of *Xbp1* mRNA splicing. Primers surrounding the region spliced out by IRE1 were used. PCR products of 140 and 114 bp, represent unspliced (*Xbp1*(u)) and spliced (*Xbp1*(s)) *Xbp1*, respectively. M, PCR molecular weight marker.

(D) Evaluation of the ratio of *Xbp1*(s) to *Xbp1*(u) by densitometry. *p<0.05, **p<0.01, ***p<0.005.

Figure 5

Δ3 GH decreases *Ghrhr* gene promoter activity.

(A) Evaluation of *Ghrhr* mRNA abundance by qRT-PCR using samples from *Gh*$^{wtGH1/wtGH1}$, *Gh*$^{wtGH1/Δ3GH1}$, *Gh*$^{-/-}$, and *Gh*$^{Δ3GH1/-}$ mice at 4 weeks old. Data presented are mean and SD values from three independent samples, with relative abundance calculated by normalization to *β-actin* expression. ***p<0.005.

(B) *In situ* hybridization evaluation of *Ghrhr* mRNA expression in pituitary glands from E19.5 and 4-week-old $Gh^{wtGH1/wtGH1}$, $Gh^{wtGH1/\Delta 3GH1}$, $Gh^{-/-}$, and $Gh^{\Delta 3GH1/-}$ mice. Scale bars, 100 μM.

(C) Growth curves of male $Gh^{-/-}$ and $Gh^{\Delta 3GH1/-}$ mice.

(D) Results of X-gal staining of pituitary glands from 4-week-old and E19.5 $Ghrhr^{+/LacZ}$; $Gh^{wtGH1/wtGH1}$ and $Ghrhr^{+/LacZ}$; $Gh^{wtGH1/\Delta 3GH1}$ mice. Arrows indicate pituitary glands. Scale bars, 2 mm.

Figure 6

Levels of nuclear CREB3L2 are decreased in pituitary glands from $Gh^{wtGH1/\Delta 3GH1}$ mice.

(A) Evaluation of Creb3 family member expression in 4-week-old whole pituitary glands by RT-PCR.

(B) Evaluation of *Creb3l1* and *Creb3l2* gene expression in pituitary glands from 4-week-old $Gh^{wtGH1/wtGH1}$ and $Gh^{wtGH1/\Delta 3GH1}$ mice by qRT-PCR. *p<0.05.

(C) Evaluation of cytoplasmic (Cy) and nuclear (N) expression levels of CREB3L1 and CREB3L2 by immunoblotting. Anterior pituitary cells from four-week-old $Gh^{wtGH1/wtGH1}$ and $Gh^{wtGH1/\Delta 3GH1}$ mice were dissociated and separated into Cy and N fractions. GAPDH and LAMIN A/C were used as positive controls for Cy and N fractions, respectively.

(D) Reporter assay to evaluate expression driven by the *Ghrhr* (500 bp) and *Gh* (400 bp) promoters using vectors expressing POU1F1, CREB3l1-N, and CREB3l2-N.

(E, F) Evaluation of CREB3L2 protein levels in pituitary glands from E19.5 mouse embryos by immunoblotting. **p<0.01.

(G) Evaluation of the abundance of *Sec23a* mRNA in pituitary glands from E19.5 mouse embryos by qRT-PCR. *p<0.05.

Figure 7

A schematic representation of Δ3 GH-mediated dominant negative effects in IGHD2 model mice.

Tables

Table 1

	wild type GH - wild type GH	wild type GH-Δ3 GH
ZDOCK score	150.6±16.58 (n=234)	146.21±19.18 (n=938)*

Results of docking simulation of wild-type and Δ3 GH. Higher ZDOCK score indicates more stable binding affinity. Numbers indicate times of the docking runs. ***p<0.001.

Expanded View Figure Legends

Expanded View Figure 1

Establishment of IGHD2 model mice using the gene exchange system.

(A) Schematic representation of the gene exchange system. Vertical long open and grey rectangles represent the open reading frames of the endogenous *Gh* and exchanged human *GH1* genes, respectively. Orange and purple rectangles represent untranslated regions of the *Gh* gene. Black bold lines represent homology arms. Red and blue bold lines represent probes used for Southern blotting to detect homologous recombination of the neoR gene and exchange of the *GH1* gene. Red and blue vertical lines represent EcoRI and KpnI recognition sites, respectively. Green arrows numbered from 1 to 4, genotyping primers. DT-A, diphtheria toxin A.

(B) Results of Southern blotting using probes indicated in (A).

(C) Intact and mutant loxP sequences used in this study; red letters indicate mutant sequences.

(D) Typical results of PCR genotyping using primers 1 to 4. Signals detecting Gh^{+}, Gh^{-}, and Gh^{wtGH1} or $Gh^{\Delta 3GH1}$ are shown. M: PCR molecular weight marker.

(E) Growth curves of male $Gh^{+/\Delta 3GH1}$ and $Gh^{mGh/\Delta 3GH1}$ mice.

(F) qRT-PCR evaluating the abundance of mRNA transcribed from the endogenous and exchanged *Gh* alleles in pituitary glands from 4-week-old mice.

Expanded View Figure 2

(A) GH4C1 cells were transfected with *wtGH1* and/or *Δ3GH1* cDNA constructs in the presence or absence of treatment with the proteasome inhibitor, MG132. Cell lysate samples were subjected to immunoblotting analysis using anti-GH antibody. Upper numbers indicate the quantities of transfected plasmid DNA, encoding either *wtGH1* or *Δ3GH1*, cDNA. Note that Δ3 GH is degraded by the proteasome and the anti-GH antibody used in this study has comparable affinities for both wild-type and Δ3 GH proteins.

(B) Evaluation of the distribution of wild-type and Δ3 GH by soluble/insoluble fraction assay. Four-week-old anterior pituitary cells from $Gh^{wtGH1/\Delta 3GH1}$ mice were dissociated, separated into soluble (S) and insoluble (I) fractions, and subjected to immunoblotting in the presence or absence of MG132 treatment (10 μM, 4 h). GAPDH was used as a

positive control for the soluble fractions.
(C) Photograph of male *Gh*$^{-/-}$, and *Gh*$^{\Delta 3GH1/-}$ mice at 8 weeks old.

Expanded View Figure 3
(A) A strategy for establishing *LacZ* knocked-in model mice, using the CRISPR/Cas9 system. The *LacZ* gene was inserted into exon 1 of the *Ghrhr* gene by homologous recombination. Blue and orange bars, 5′ and 3′ homology arm CRISPR oligonucleotides, respectively. Purple bar, probe used for Southern blotting. NLS, nuclear-localization signal; B, BglII recognition site.
(B) Results of Southern blotting using the probe indicated in (A).
(C) Evaluation of cytoplasmic and nuclear POU1F1 expression levels by immunoblotting. Anterior pituitary cells from four-week-old *Gh*$^{wtGH1/wtGH1}$ and *Gh*$^{wtGH1/\Delta 3GH1}$ mice were dissociated, separated into cytoplasmic (Cy) and nuclear (N) fractions, and subjected to immunoblotting analysis. GAPDH and LAMIN A/C were used as positive controls for Cy and N fractions, respectively.
(D) Evaluation of wild-type GH, CREB3L1, and CREB3L2 expression in pituitary glands from 4-week-old *Gh*$^{wtGH1/wtGH1}$ and *Gh*$^{wtGH1/\Delta 3GH1}$ mice by immunofluorescence analysis.

Figure 1

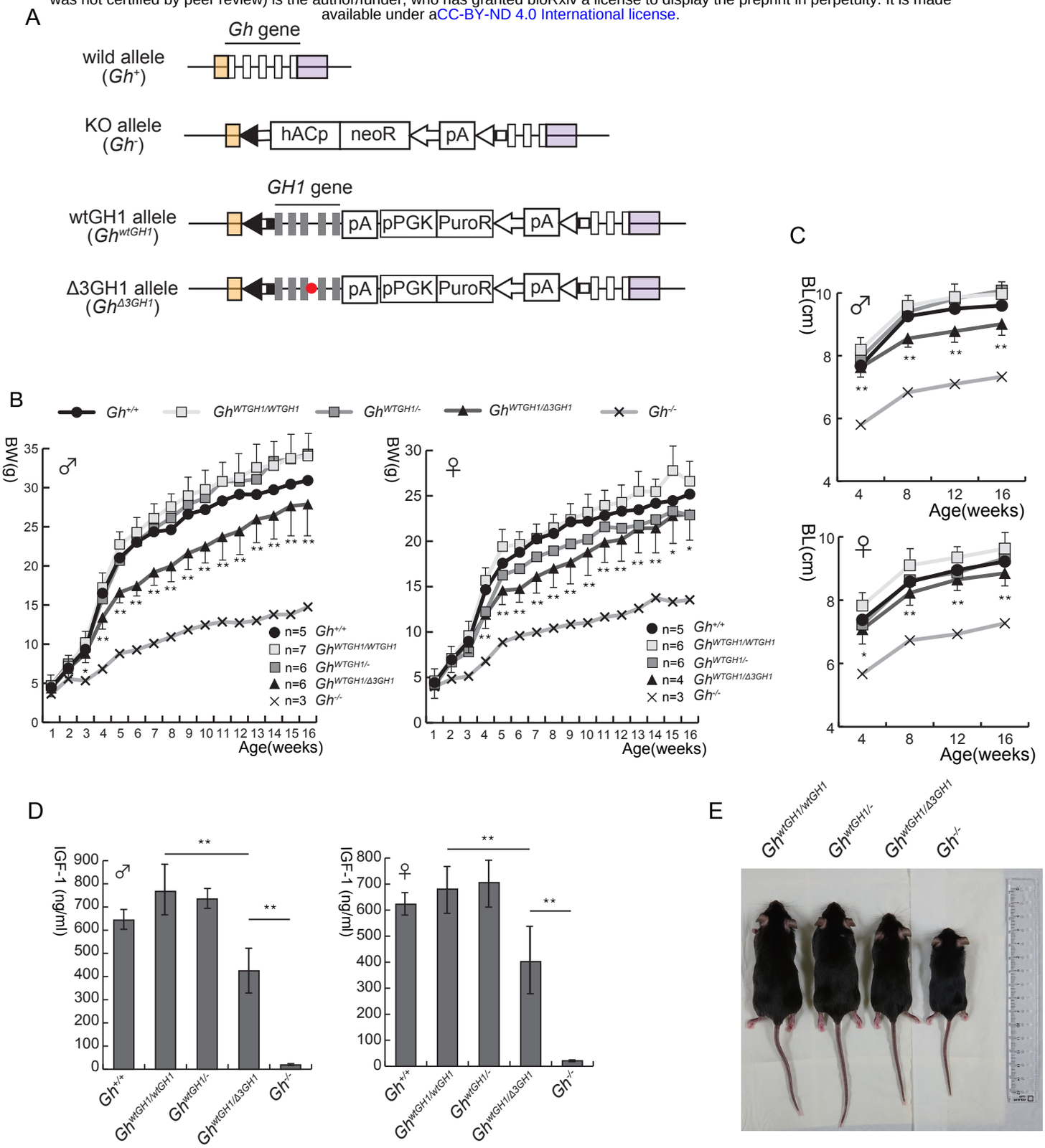

Figure 2

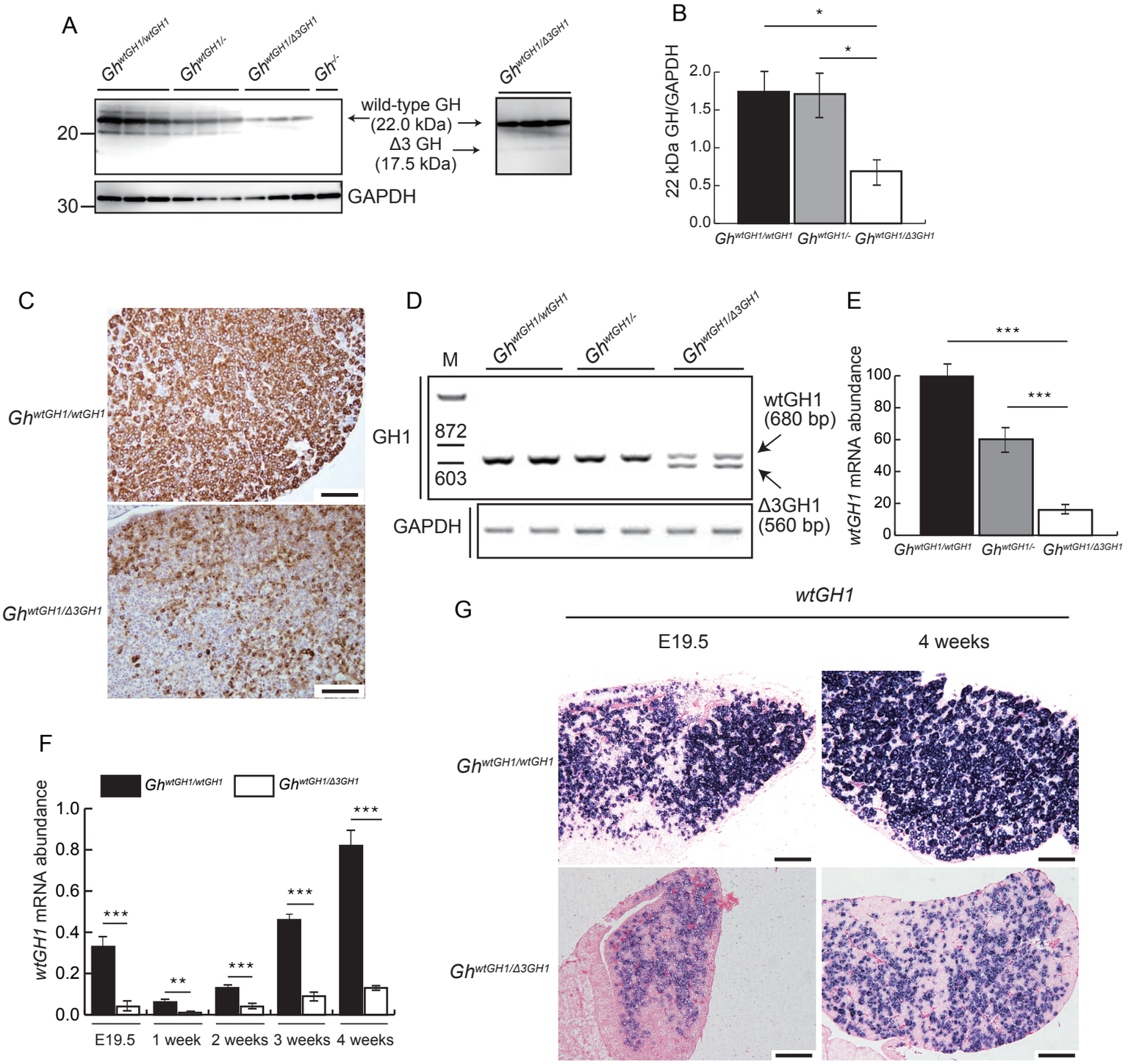

Figure 3

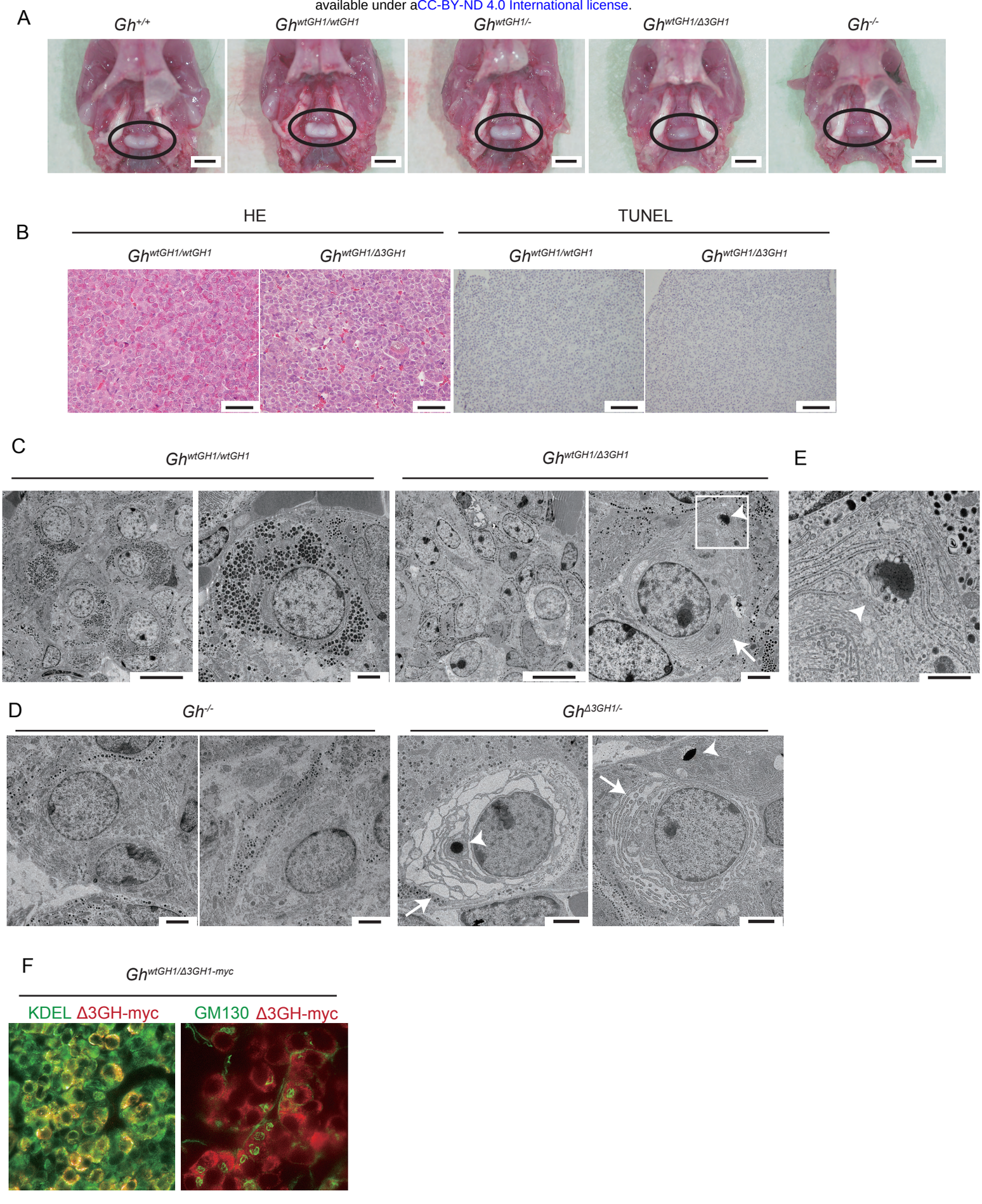

Figure 4

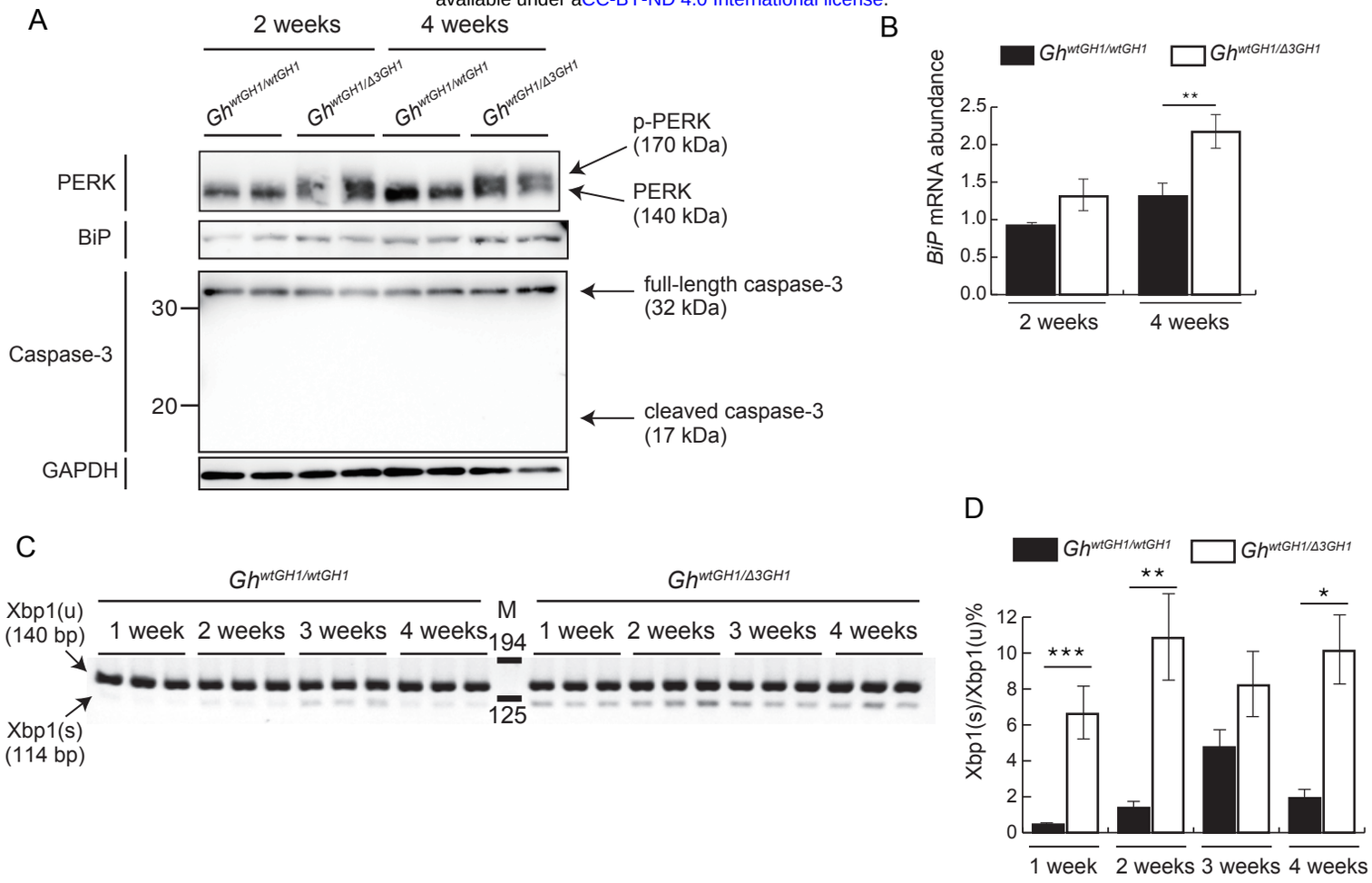

Figure 5

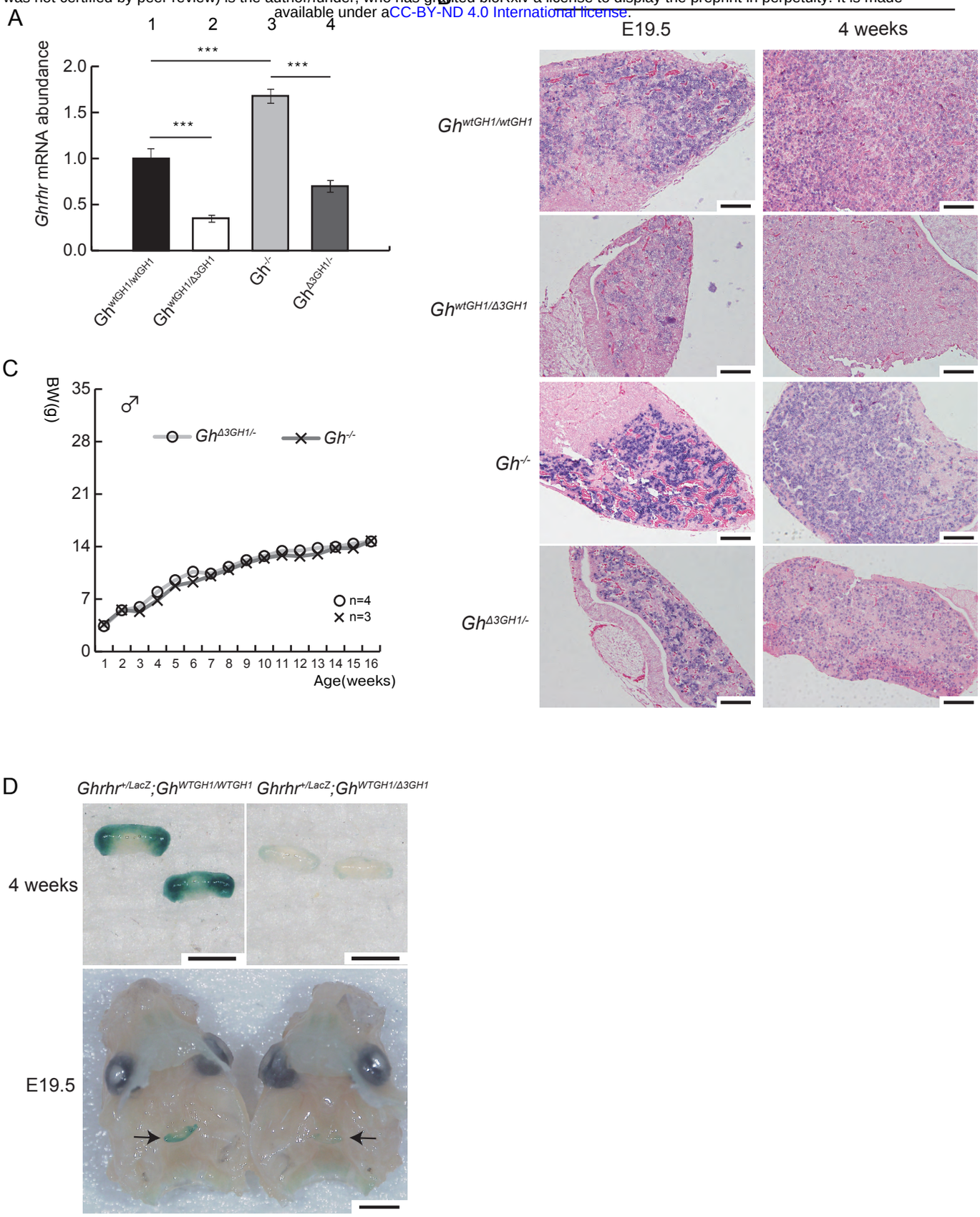

Figure 6

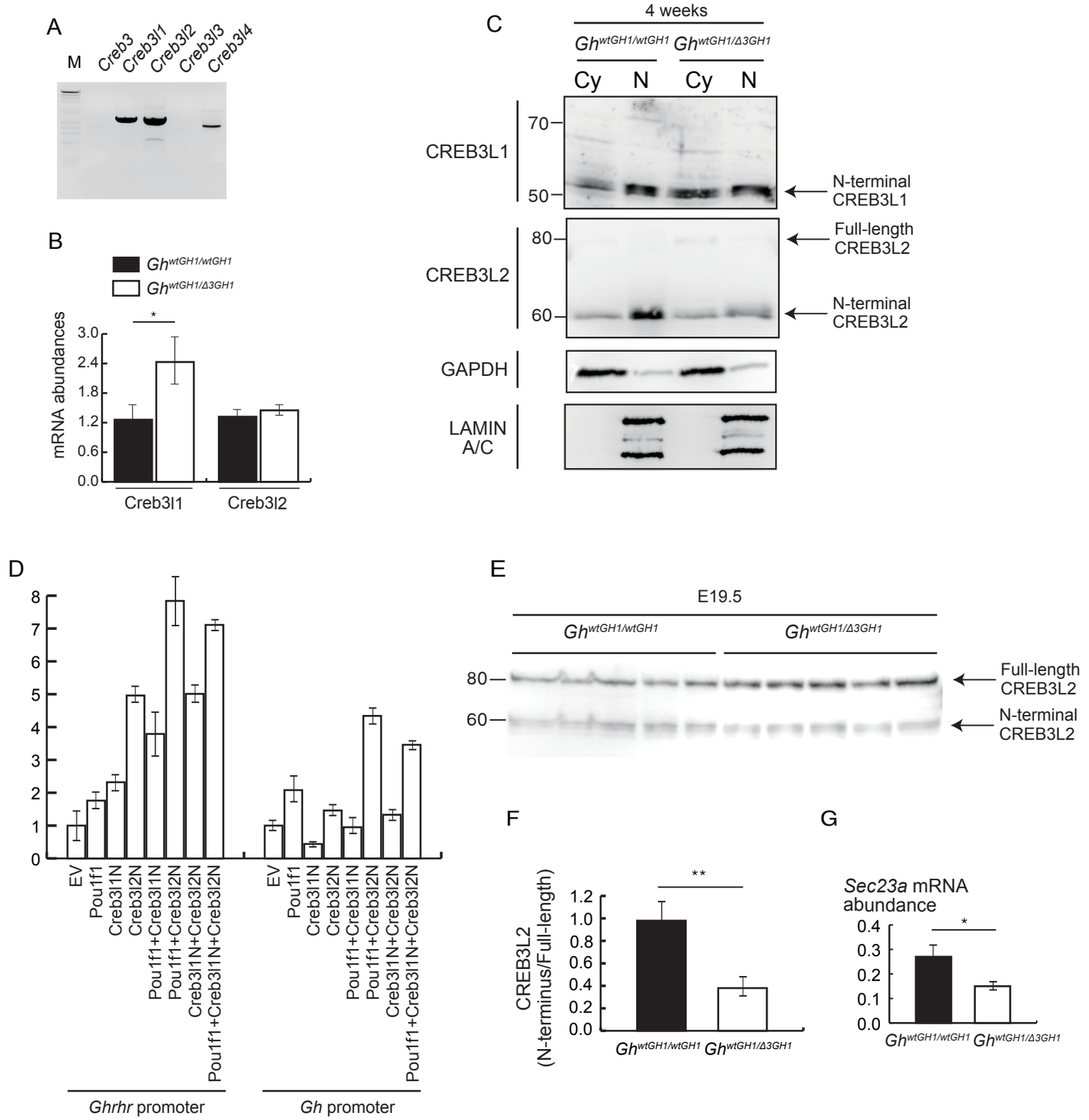

Figure 7

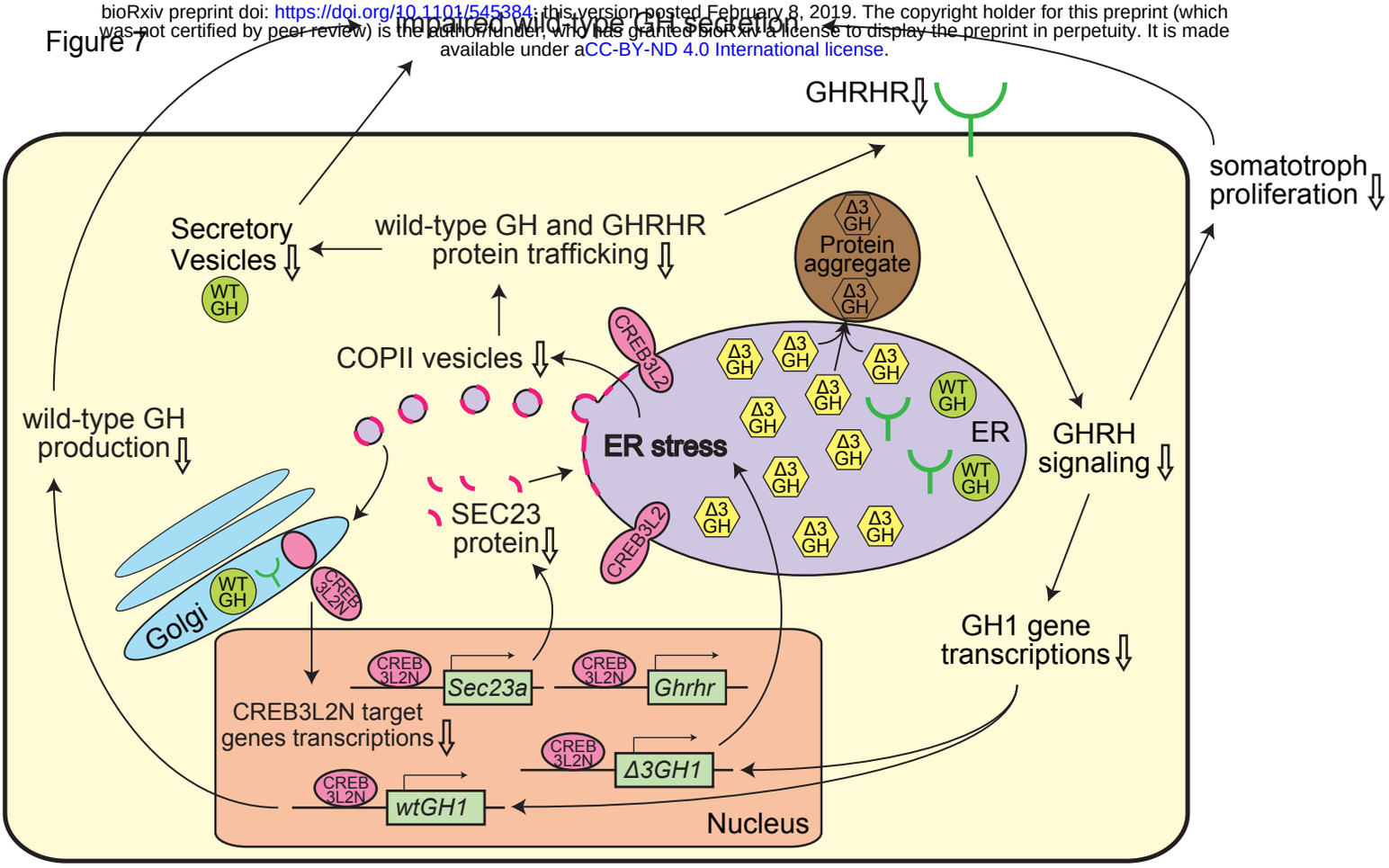

Expanded View Figure 1

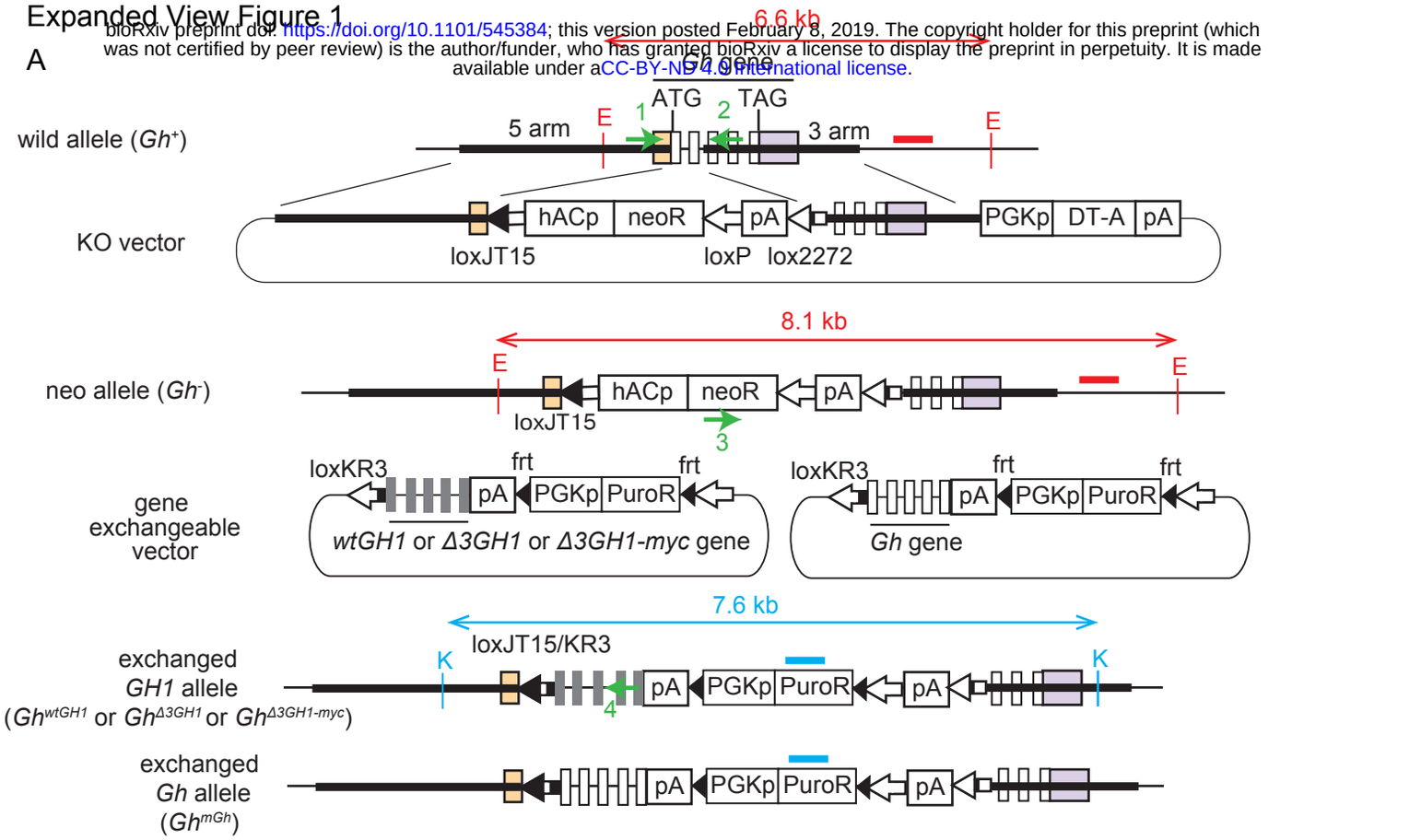

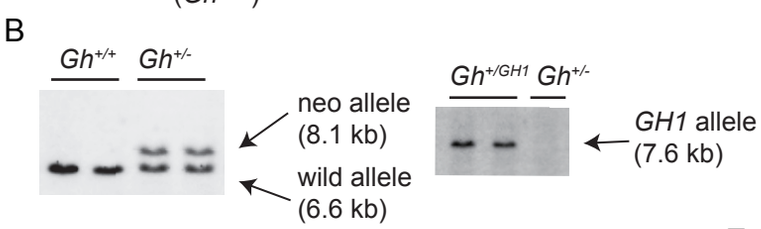

C

loxP	ATAACTTCGTATAGCATACATTATACGAAGTTAT
loxJT15	AATTATTCGTATAGCATACATTATACGAAGTTAT
loxKR3	ATAACTTCGTATAGCATACATTATACCTTGTTAT

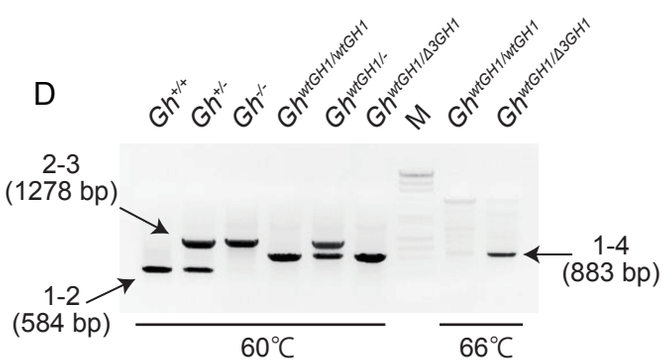

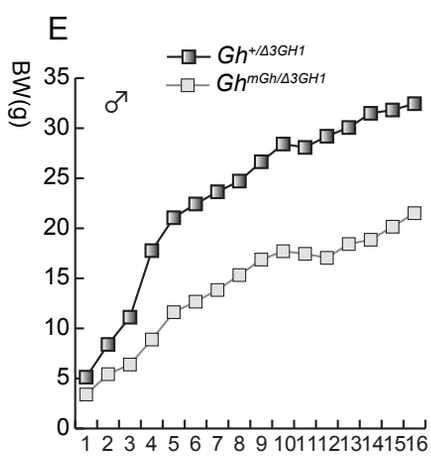

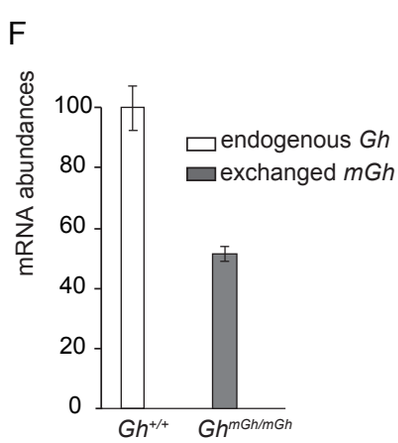

Expanded View Figure 2

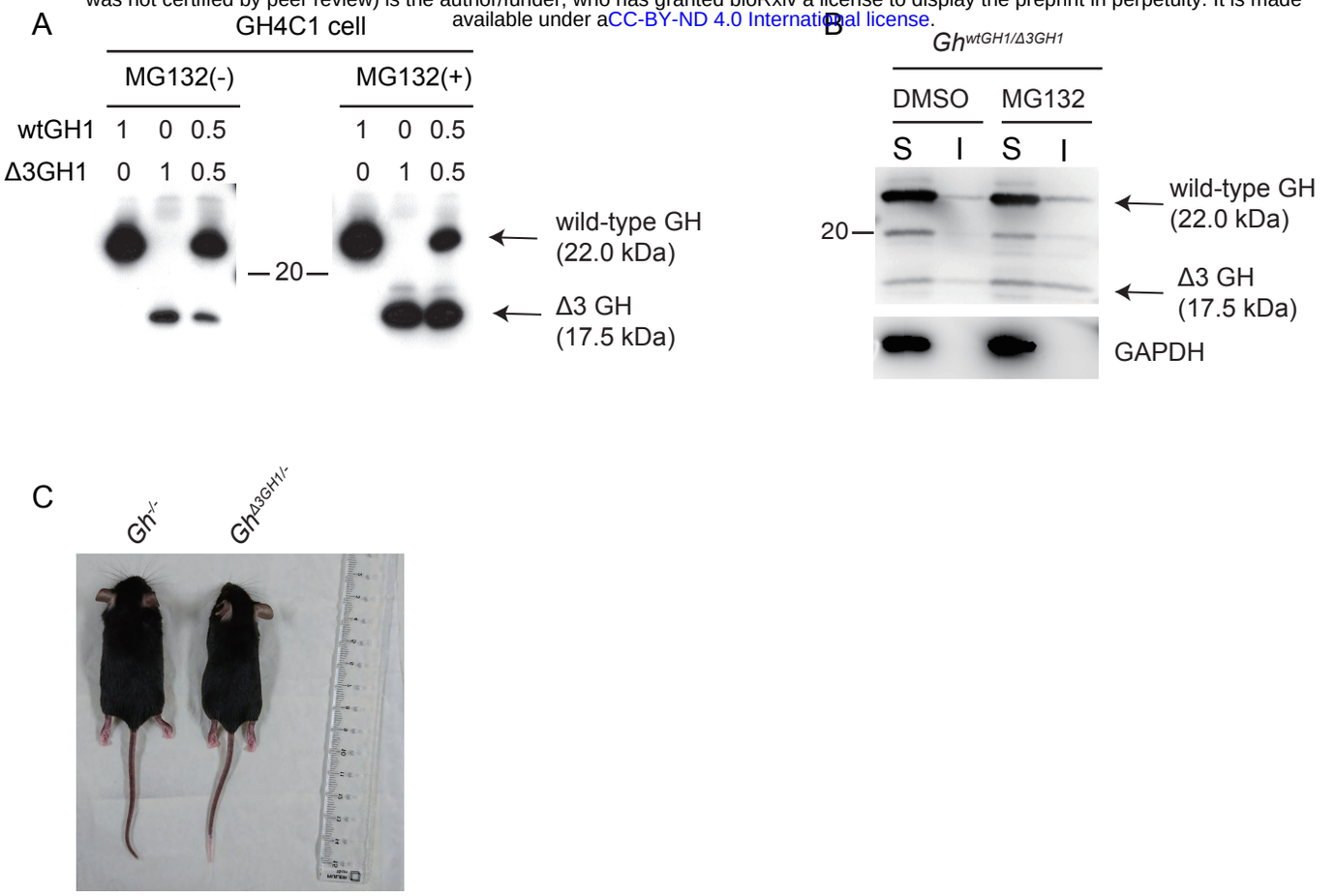

Expanded View Figure 3

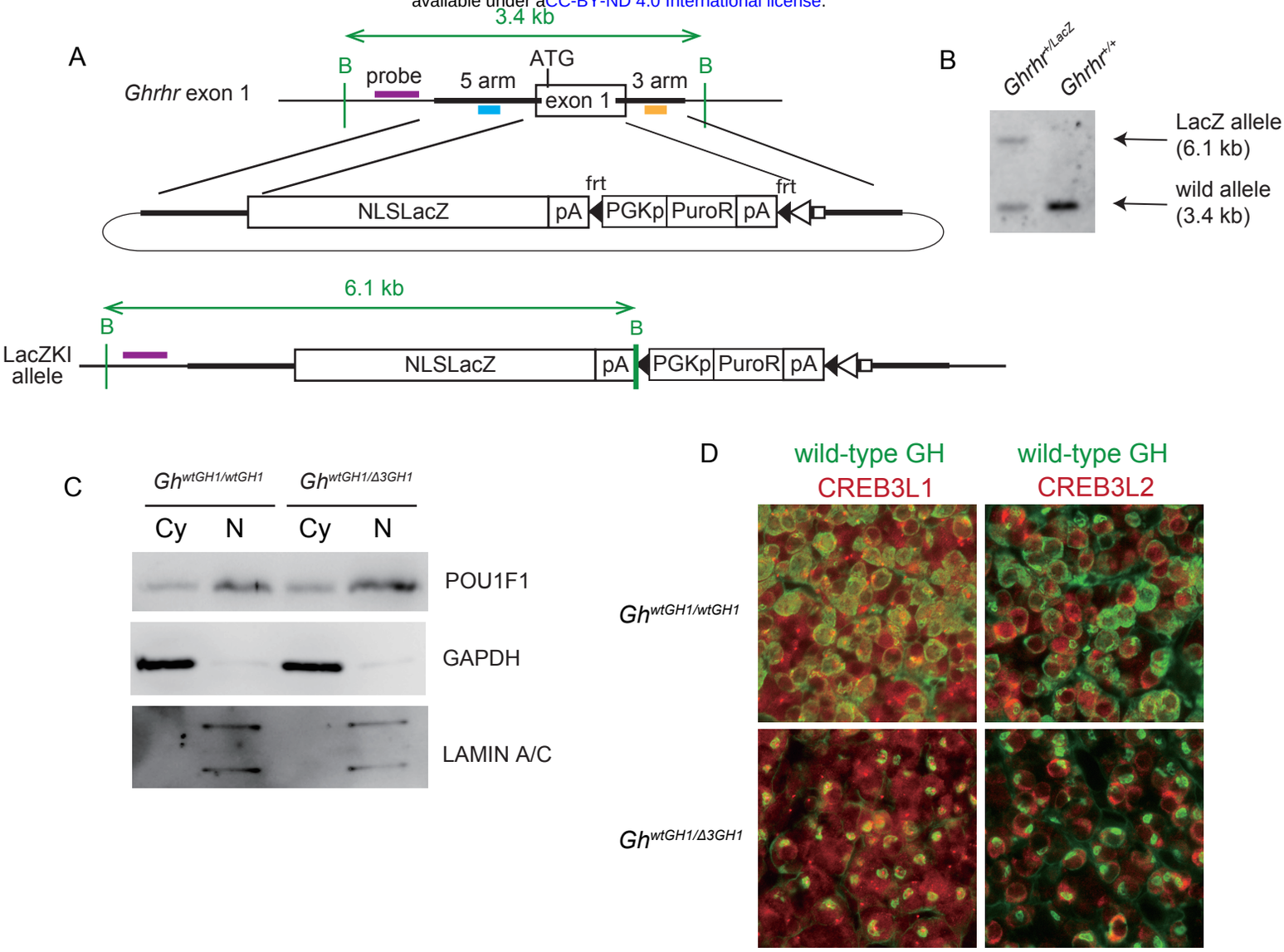

Supplementary table 1

Sequences of primers used in this study.

Primer 1	AGTCCAGATTCCAAACTGCT
Primer 2	AAGAAGGGTGGTCACTGAGG
Primer 3	AGAGGCTATTCGGCTATGAC
Primer 4	CCCTCTTCCGTAGGTGAGTA
Gh-5arm-F	AGCAGGGAGCTCTCATCGCGAGTCACTGGAACATTG
Gh-5arm-R	CATTGCCGAGCTCTGATCTGTCCACAGGACTCTG
Gh-3arm-F	AGTAATGATGTCGACGAGACACAAGCTG
Gh-3arm-R	ATATATGCAGGTCGACATAGAGACCAGAAG
GH1-gf1	GCTGTCGACAGCTCACCTAGC
GH1-gr1	TAGGAATTCCTAGAAGCCACAGCTGCCCTCCACAGAG
GH1IVS3-F	CCCAGGCGGGGATGGGGGA
GH1IVS3dsmut-R	GAGAAGGCATCCACTCACGGATT
GH1-cf1	TCCTGTGGACAGCTCACCTAG
GH1-cr1	CTAGAAGCCACAGCTGCCCT
GH1ex3-f1	TTCAGATCTGAAGAAGCCTATATCCCAAAG
GH1ex3-r1	TCCGATATCGGATTTCTGTTGTGTTTCCTC
Ghrhr-5arm-f5	TTCTCGTTGGAATTCTCAGCTCACCCTC
Ghrhr-5arm-r5	AATGGTGTCTGAATTCAGCCTTCCCTC
Ghrhr-3arm-f6	CAGACCTTTGTTCTCGAGGGTGGTGGCAG
Ghrhr-3arm-r6	CAGAGGCAAACGAAAGCTCGAGTCACAG
Ghrhr-vf1	CATAGATCTATGGATGGCCTGATGTGGGC
Ghrhr-vr1	TAGCTCGAGCTAGCACTCAGAGGTCAGCA
Ghrhr-CRI-f1	CACCGAGTAAGGCTATTGGTGAAC
Ghrhr-CRI-r1	AAACGTTCACCAATAGCCTTACTC
Ghrhr-CRI-f2	CACCAGAAACCAGCTACTGCTCCC
Ghrhr- CRI-r2	AAACGGGAGCAGTAGCTGGTTTCT
Ghrhr-CRI-f4	CACCGGATCAAAGTCACTCAGAGA
Ghrhr-CRI-r4	AAACTCTCTGAGTGACTTTGATCC
Ghrhr-CRI-f5	CACCCTCTCTCTGGGACTCACACC
Ghrhr-CRI-r5	AAACGGTGTGAGTCCCAGAGAGAG
Xbp1-f1	AGGCCAAGGGGAGTGGAGTA
Xbp1-r1	AGGCAACAGTGTCAGAGTCC
wtGH1-qf1	AGCCTATATCCCAAAGGAAC
wtGH1-qr1	AGCAGCTCTAGGTTGGATTT
Ghrhr-qf1	TCTCTCACTTCGGCTCAGACAC
Ghrhr-qr1	TCTTCACCGTGGAGAAGTACGA
Actb-qf1	TCTGTGTGGATCGGTGGCTCCA
Actb-qr1	CCTGCTTGCTGATCCACATCTG
WZ-14	GCTCTCTACAGGTGGATCAAG
WZ-17	GCAGTTCAATCAGCTGCTTTC
Hspa5-qf2	AACTGTAACAATCAAGGTCT
Hspa5-qr2	CAAAAGTGACTTCAATCTGG
Pou1f1-vf1	CATGGTACCATGAGTTGCCAATCTTTCACCTC
Pou1f1-vr1	TAAGGTACCTTATCTGCACTCTAGATGTTCC
Creb3l1-vf1	CATGGTACCATGGACGCCGTCTTGGAACC
Creb3l1-vr1	TAGGGTACCCTAGGAGAGTTTGATGGTGG
Creb3l1 ex2-1	UUUCUUUGAUGACCCUGUGCGUUUUAGAGCUAUGCUGUUUUG
Creb3l1 ex2-2	GAGCACAGCUACUCCCUGAGGUUUUAGAGCUAUGCUGUUUUG
Creb3l2-vf1	CATGAATTCATGGAGGTGCTGGAGAGCGG
Creb3l2-vr1	TGAGAATTCTCAGAAGGTGGCGTTCACTCT
Luman-cf1	CATGAATTCATGGATCCTGGTGGTCAGGAT
Luman-cr1	TAGGAATTCTAACCTGAATACCTGCCCTG
CrebH-cf1	CATAGATCTATGGATGGGGACATAGCGGCT
CrebH-cr1	TGAAGATCTTCACAGCACCCCCAATGCATC
loxP-CRIf1	AGGGGTATGCTATACGAAGTTATT
loxP-CRIr1	AAACAATAACTTCGTATAGCATAC